Eur. Phys. J. C (2017) 77:138
DOI 10.1140/epjc/s10052-017-4684-1

THE EUROPEAN PHYSICAL JOURNAL C

Regular Article - Theoretical Physics

Revisiting T2KK and T2KO physics potential and ν_μ–$\bar{\nu}_\mu$ beam ratio

Kaoru Hagiwara[1,2,a], **Pyungwon Ko**[3,b], **Naotoshi Okamura**[4,c], **Yoshitaro Takaesu**[5,d]

[1] Theory Center, KEK, 1-1 Oho, Tsukuba, Ibaraki 305-0801, Japan
[2] Department of Accelerator Science, Sokendai, 1-1 Oho, Tsukuba, Ibaraki 305-0801, Japan
[3] School of Physics, KIAS, 85 Hoegi-ro, Dongdaemun-gu, Seoul 130-722, Korea
[4] Department of Radiological Sciences, International University of Health and Welfare, 2600-1 Kitakanemaru, Ohtawara, Tochigi 324-8501, Japan
[5] Department of Physics, University of Tokyo, Tokyo 113-0033, Japan

Received: 1 June 2016 / Accepted: 8 February 2017

Abstract We revisit the sensitivity study of the Tokai-to-Kamioka-and-Korea (T2KK) and Tokai-to-Kamioka-and-Oki (T2KO) proposals where a water Čerenkov detector with the 100 kton fiducial volume is placed in Korea (L = 1000 km) and Oki island (L = 653 km) in Japan, respectively, in addition to the Super-Kamiokande for determination of the neutrino mass hierarchy and leptonic CP phase ($\delta_{\rm CP}$). We systematically study the running ratio of the ν_μ and $\bar{\nu}_\mu$ focusing beams with dedicated background estimation for the ν_e appearance and ν_μ disappearance signals, especially improving treatment of the neutral-current π^0 backgrounds. Using a ν_μ–$\bar{\nu}_\mu$ beam ratio between 3:2 and 2.5:2.5 (in units of 10^{21}POT with the proton energy of 40 GeV), the mass-hierarchy determination with the median sensitivity of 3–5 σ by the T2KK and 1–4 σ by the T2KO experiment are expected when $\sin^2\theta_{23} = 0.5$, depending on the mass-hierarchy pattern and CP phase. These sensitivities are enhanced (reduced) by 30–40% in $\Delta\chi^2$ when $\sin^2\theta_{23} = 0.6\,(0.4)$. The CP phase is measured with the uncertainty of 20°–50° by the T2KK and T2KO using the ν_μ–$\bar{\nu}_\mu$ focusing beam ratio between 3.5:1.5 and 1.5:3.5. These findings indicate that inclusion of the $\bar{\nu}_\mu$ focusing beam improves the sensitivities of the T2KK and T2KO experiments to both the mass-hierarchy determination and the leptonic CP phase measurement simultaneously with the preferred beam ratio being between 3:2–2.5:2.5 ($\times 10^{21}$POT).

1 Introduction

After the accurate measurements of $\sin^2 2\theta_{13}$ by DayaBay [1–6], Reno [7,8] and Double Chooz [9–13] experiments, determination of the neutrino mass hierarchy and CP violating phase in the Maki–Nakagawa–Sakata (MNS) mixing matrix [14] has been the next targets in neutrino physics.

Ideas of extending the Tokai-to-Kamioka (T2K) experiment with additional water Čerenkov detectors placed in Korea (Tokai-to-Kamioka-and-Korea, T2KK, experiment [15–26]) or in Oki island (Tokai-to-Kamioka-and-Oki, T2KO, experiment [25,27]) have been proposed to address those questions.[1] It has been shown that the T2KK experiment with a 100 kton fiducial-volume detector in Korea in addition to the SK detector is an appealing proposal if we can use the J-PARC neutrino beam with 0.64 MW beam power and the 2.5°–3.0° off-axis angle at the SK [17,18,20,22,24]. The authors of Ref. [17,18,20] investigated the sensitivities to the mass hierarchy and CP phase with the ν_μ focusing beam in a simple manner, ignoring the effects of neutral-current (NC) π^0 backgrounds, miss-identification of a muon as an electron, and smearing of reconstructed neutrino energy. Authors of Ref. [22] then re-evaluated the physics potential of the same T2KK setup with careful consideration on those effects.

Inclusion of $\bar{\nu}_\mu$ focusing beams may improve the sensitivity of long-baseline oscillation experiments to the mass hierarchy since the matter effects, which enhance the mass-hierarchy difference in neutrino oscillation patterns, appear in the opposite way in ν_μ and $\bar{\nu}_\mu$ oscillations. The impacts of including the $\bar{\nu}_\mu$ focusing beam in the T2KK experiment was studied in Ref. [24]. The authors considered the running

[1] For the CP phase measurement, there are also proposals to utilize neutrinos from muon decays at rest [28–30].

[a] e-mail: kaoru.hagiwara@kek.jp
[b] e-mail: pko@kias.re.kr
[c] e-mail: nokamura@iuhw.ac.jp
[d] e-mail: takaesu@hep-th.phys.s.u-tokyo.ac.jp

Published online: 01 March 2017

ratio of the ν_μ and $\bar{\nu}_\mu$ focusing beams of 5:0 and 2.5:2.5 in the units of protons on target (POT) and argued that including the $\bar{\nu}_\mu$ focusing beam improves the sensitivity to the mass-hierarchy determination significantly. The impact of anti-neutrino beams was also studied in Ref. [16] for a different T2KK setup; two 270 kton detectors are each placed at Kamioka and Korea, receiving 2.5° off-axis beams with the beam power of 4 MW and the total running time of 8 years. The physics potential of the T2KO experiment was also investigated [25] with a similar analysis and conclusion as in Ref. [24]. However, those studies again did not consider the effects of the NC π^0 backgrounds, miss-identified muon, and events from other neutrino–nucleus interactions than the charged-current quasi-elastic (CCQE) one. Therefore, it is not very clear whether the ν_μ–$\bar{\nu}_\mu$ focusing beam ratio of 1:1 is the best for the mass-hierarchy determination and CP phase measurement.

In this paper, we revisit the sensitivity study of the T2KK [22,24] and T2KO [25] experiments for the neutrino mass hierarchy and CP phase, studying the dependence of the sensitivities on the ν_μ–$\bar{\nu}_\mu$ focusing beam ratio systematically with dedicated estimation of backgrounds. Especially, the treatment of the NC π^0 backgrounds is improved in this analysis. The NC π^0 backgrounds is estimated using a realistic π^0 rejection probability based on the POLfit (Pattern Of Light fitter) algorithm [31], and the contribution form the coherent π^0 production process is taken into account, which is neglected in the previous analysis [22]. The uncertainty of the NC π^0 backgrounds is also reconsidered including the uncertainty from the axial masses in the models of neutrino–nucleus scattering cross sections [32,33].

The remaining part of this paper is organized as follows. After describing the T2KK and T2KO experimental setups in Sect. 2, our analysis details are discussed in Sect. 3. Results for the sensitivity of the T2KK and T2KO experiments to the mass-hierarchy determination and CP phase measurements are presented in Sects. 4 and 5, and our main conclusions are summarized in Sect. 6.

2 Simulation details of T2KK and T2KO experiments

In this section, we fix our notation and introduce useful approximated formulas for the $\nu_\mu \to \nu_\mu$ and $\nu_\mu \to \nu_e$ oscillation probabilities. We then describe the experimental setups and discuss the simulation details of the expected signal event number in those experiments, taking into account of smearing of reconstructed neutrino energy due to the Fermi motions of target nuclei, detector resolution and contamination of events from non-CCQE neutrino–nucleus interactions. Simulation of the background events are also discussed: the NC single-π^0 background and its uncertainty, the secondary neutrino beam backgrounds, and miss-identified muon/electron backgrounds.

2.1 Neutrino oscillations in matter

We briefly review the neutrino oscillation probabilities in matter, presenting analytic approximations for the $\nu_\mu \to \nu_\mu$ (ν_μ disappearance) and $\nu_\mu \to \nu_e$ (ν_e appearance) oscillation modes, which are useful for understanding the physics potential of the T2KK and T2KO experiments qualitatively.

We work in the three neutrino flavor scheme, where the neutrino flavor eigenstate $|\nu_\alpha\rangle$ ($\alpha = e, \mu, \tau$) are mixtures of the three mass eigenstates $|\nu_i\rangle$ with their masses m_i ($i = 1, 2, 3$) as

$$|\nu_\alpha\rangle = \sum_{i=1}^{3} U_{\alpha i} |\nu_i\rangle. \tag{2.1}$$

Here U is the Maki–Nakagawa–Sakata (MNS) [14] matrix, which can be parameterized with the three mixing angles, $\theta_{12}, \theta_{13}, \theta_{23}$, and three phases, $\delta_{\rm CP}, \phi_1, \phi_2$ [34]. Among them, two phases can be eliminated in lepton number conserving processes, remaining one relevant phase, $\delta_{\rm CP}$, to neutrino oscillation experiments. The definition regions of the four parameters are chosen as $0 \le \theta_{12}, \theta_{13}, \theta_{23} \le \pi/2$, and $-\pi \le \delta_{\rm CP} \le \pi$.

The probability that an initial flavor eigenstate $|\nu_\alpha\rangle$ with energy E is observed as a flavor eigenstate $|\nu_\beta\rangle$ after traveling a distance L in the matter of density $\rho(x)$ ($0 < x < L$) is given by

$$P_{\nu_\alpha \to \nu_\beta} = \left| \langle \nu_\beta | \exp\left(-i \int_0^L H(x) \mathrm{d}x \right) |\nu_\alpha\rangle \right|^2, \tag{2.2}$$

where the Hamiltonian inside matter is

$$\begin{aligned} H(x) &= \frac{1}{2E} U \begin{pmatrix} 0 & 0 & 0 \\ 0 & \delta m_{21}^2 & 0 \\ 0 & 0 & \delta m_{31}^2 \end{pmatrix} U^\dagger + \frac{a(x)}{2E} \begin{pmatrix} 1 & 0 & 0 \\ 0 & 0 & 0 \\ 0 & 0 & 0 \end{pmatrix} \\ &= \frac{1}{2E} \tilde{U}(x) \begin{pmatrix} \lambda_1(x) & 0 & 0 \\ 0 & \lambda_2(x) & 0 \\ 0 & 0 & \lambda_3(x) \end{pmatrix} \tilde{U}^\dagger(x) \end{aligned} \tag{2.3}$$

with $\delta m_{ij} \equiv m_i^2 - m_j^2$. $a(x)/2E$ is the effective potential due to electrons in matter as

$$\begin{aligned} a(x) &= 2\sqrt{2} G_F E n_e(x) \\ &\simeq 7.56 \times 10^{-5} [\mathrm{eV}^2] \left(\frac{\rho(x)}{\mathrm{g/cm}^3} \right) \left(\frac{E}{\mathrm{GeV}} \right), \end{aligned} \tag{2.4}$$

where G_F is the Fermi constant and $n_e(x)$ is the electron number density. In the translation from $n_e(x)$ to $\rho(x)$, we assume that the number of the neutrons in matter is the same as that of protons. $\lambda_i(x)/2E$ and $\tilde{U}(x)$ are the eigenvalues and the corresponding unitary matrix of the Hamiltonian at the distance x, respectively. To a good approximation [24,

35,36], the matter density along the T2K, T2KO and T2KK baselines can be replaced by the averaged one, $\rho(x) \simeq \bar{\rho}$, and so as $a(x)$ in Eq. (2.3), $a(x) \simeq \bar{a}$. Then the oscillation probability, $P_{\nu_\alpha \to \nu_\beta}$, can be expressed compactly by using x-independent eigenvalues, λ_i, and a unitary matrix, $\tilde{U}$, as

$$P_{\nu_\alpha \to \nu_\beta} = \delta_{\alpha\beta} - 4 \sum_{i>j} \mathrm{Re}(\tilde{U}^*_{\alpha i} \tilde{U}_{\beta i} \tilde{U}_{\alpha j} \tilde{U}^*_{\beta j}) \sin^2 \frac{\tilde{\Delta}_{ij}}{2} - 2 \sum_{i>j} \mathrm{Im}(\tilde{U}^*_{\alpha i} \tilde{U}_{\beta i} \tilde{U}_{\alpha j} \tilde{U}^*_{\beta j}) \sin \tilde{\Delta}_{ij}, \quad (2.5a)$$

$$\tilde{\Delta}_{ij} \equiv \frac{\lambda_i - \lambda_j}{2E} L\,. \quad (2.5b)$$

Our numerical results are based on the above solution, Eq. (2.5a), and the main results are not affected significantly by the matter density profile as long as the mean matter density is chosen appropriately [24,25].

In this study we are mainly interested in the $\nu_\mu \to \nu_e$ and $\nu_\mu \to \nu_\mu$ oscillation modes and their charge conjugated ones. It is useful to write them down in the approximated analytic forms as [17]

$$P_{\nu_\mu \to \nu_\mu} \simeq 1 - \sin^2 2\theta_{\mathrm{atm}} \{(1 + A^\mu) \sin^2 \Delta_{31} + B^\mu \sin(2\Delta_{31})\} + C^\mu, \quad (2.6a)$$

$$P_{\nu_\mu \to \nu_e} \simeq 4 \sin^2 \theta_{13} \sin^2 \theta_{23} \{(1 + A^e) \sin^2 \Delta_{31} + B^e \sin(2\Delta_{31})\} + C^e, \quad (2.6b)$$

where $\sin\theta_{\mathrm{atm}} \equiv \sin\theta_{23}\cos\theta_{13}$ and $\Delta_{ij} \equiv \delta m^2_{ij} L/4E$. Here A^α, B^α, and $C^\alpha (\alpha = \mu, e)$ are corrections due to the matter effect and the smaller mass difference δm^2_{21}:

$$A^\mu \simeq 0, \quad (2.7a)$$

$$B^\mu \simeq \Delta_{21} \cos^2\theta_{12}, \quad (2.7b)$$

$$C^\mu \simeq 0, \quad (2.7c)$$

$$A^e \simeq \frac{aL}{2\Delta_{31}E} - \Delta_{21} \frac{\sin 2\theta_{12}}{\tan\theta_{23} \sin\theta_{13}} \sin\delta_{\mathrm{CP}}, \quad (2.7d)$$

$$B^e \simeq -\frac{aL}{4E} + \frac{\Delta_{21}}{2} \frac{\sin 2\theta_{12}}{\tan\theta_{23} \sin\theta_{13}} (\cos\delta_{\mathrm{CP}} - 2\sin^2\theta_{12}), \quad (2.7e)$$

$$C^e \simeq \Delta^2_{21} \sin^2 2\theta_{12} \cos^2\theta_{23}. \quad (2.7f)$$

In these expressions we retain up to the sub-leading terms of Δ_{21}, $\sin^2\theta_{13}$ and $aL/4E$. The corresponding probabilities for anti-neutrino oscillations can be obtained from the above expressions by reversing the sign of the matter effect term ($a \to -a$) and the CP phase ($\delta_{\mathrm{CP}} \to -\delta_{\mathrm{CP}}$). These expressions are valid as long as those three parameters are negligibly smaller than unity; this is the case for T2K, T2KO and T2KK experiments, where typically $L/E \sim \mathcal{O}(10^2 - 10^3)[1/\mathrm{eV}^2]$.

The ν_e appearance mode plays a more important role in determining the mass hierarchy (i.e., the sign of Δ_{31}) than the ν_μ disappearance mode. This is because the appearance mode may have sensitivity to the mass hierarchy around oscillation peaks through the A^e parameter, while the disappearance mode is lack of sensitivity around oscillation peaks since $A^\mu \simeq 0$. On the other hand, the disappearance mode is important in constraining the θ_{23} mixing angle, which still has large uncertainty [34]. The ν_e appearance mode also has sensitivity to the CP phase. It is sensitive to the sine of δ_{CP} around the oscillation peaks, mainly through the A^e parameter; on the other hand, it is sensitive to the cosine of δ_{CP} between oscillation maxima and minima, mainly through the B^e parameter. Therefore, if we try to obtain the full information of the δ_{CP}, it is not enough to observe just around the first oscillation peak, as we will see later.

2.2 Experimental setups

We use the ν_μ and $\bar{\nu}_\mu$ focusing beam fluxes from the J-PARC with the proton energy of 40 GeV [37]. In Fig. 1, we show the fluxes corresponding to 10^{21} POT (protons on target) at the SK. The ν_μ ($\bar{\nu}_\mu$) focusing beams include the primary, ν_μ ($\bar{\nu}_\mu$), and secondary, $\bar{\nu}_\mu$ (ν_μ), ν_e, $\bar{\nu}_e$, components, and we take them into account in our analyses.

The baseline length from the J-PARC to the SK and Oki detectors are taken to be 295 km [38] and 653 km [25], respectively. The baseline length to a detector in Korea (Kr detector) can be taken from 1000 to 1300 km in South Korea [16,17]. In this study, we place a Kr detector at the shortest baseline length, $L = 1000$ km, to receive the J-PARC neutrino beams with the smallest off-axis angle [17], which is preferred in terms of the sensitivity to the mass-hierarchy determination [17,18,22,25]. For the nominal 2.5° off-axis angle at the SK, a Kr detector receives the ∼1° off-axis beam (OAB); the case of 3.0° OAB at the SK is also investigated, corresponding to the 0.5° OAB at a Kr detector [25]. On the other hand, variation of the off-axis angle does not affect sensitivities of the T2KO experiment to the mass hierarchy and CP phase measurements significantly [25], and we only consider the 2.5° off-axis angle at the SK for the T2KO experiment, corresponding to 0.9° OAB at the Oki detector [25].

The averaged matter densities, $\bar{\rho}$, along the baseline between J-PARC and SK, Oki or Kr detectors, have been evaluated in Refs. [24,25] and taken as in Table 1 in this study. It is sufficient to use those averaged densities in those long-baseline neutrino experiments [24], and we neglect small effects from the variation of the matter density along those baselines.

2.3 Signal events

In this subsection we describe how to estimate the signal event numbers at the SK, Oki, and Korea detectors. We consider charged-current quasi-elastic (CCQE) events, $\nu_l\, n \to l\, p$ or $\bar{\nu}_l\, p \to \bar{l}\, n$ ($l = \mu$ or e), from the $\nu_\mu \to \nu_\mu$ and $\nu_\mu \to \nu_e$ oscillation modes and their charge conjugated

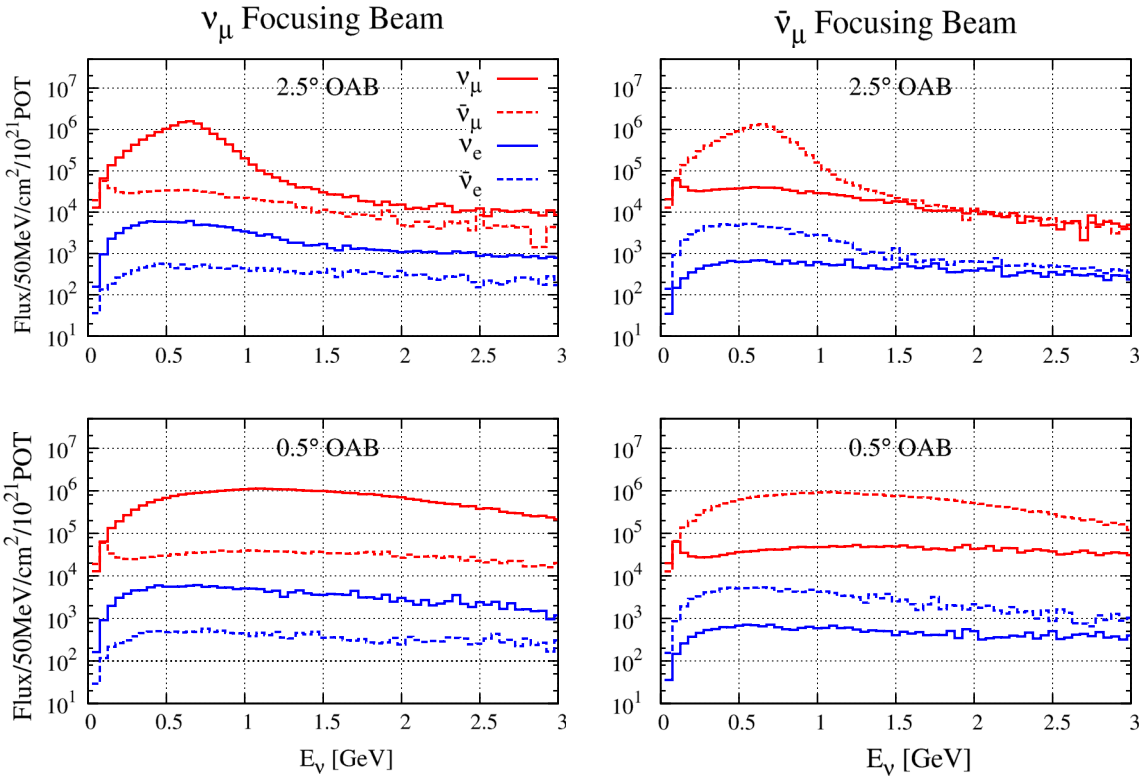

Fig. 1 The neutrino fluxes in ν_μ and $\bar{\nu}_\mu$ focusing beams at the SK as functions of neutrino energy. The *left* and *right plots* are for the ν_μ and $\bar{\nu}_\mu$ focusing beams, while the *upper* and *lower plots* are for the 2.5° and 0.5° off-axis beams (OAB), respectively. In each plot, the fluxes of ν_μ (*solid red*), $\bar{\nu}_\mu$ (*dashed-red*), ν_e (*solid-blue*), and $\bar{\nu}_e$ (*dashed-blue*) are shown. The fluxes are normalized to 10^{21} POT with 40 GeV proton energy

Table 1 Summary of the parameters related to detectors at Kamioka (SK), Oki island (Oki) and Korea (Kr). L is the baseline length between the J-PARC and a detector, FV is the fiducial volume of a detector, $\bar{\rho}$ is the average matter density along a baseline, and OA is the off-axis angle of the J-PARC neutrino (anti-neutrino) beams at a detector. The first and second OA angles at the Oki and Kr detectors are related to the corresponding OA angles at the SK. These parameter values are used as default in our simulation unless otherwise mentioned

Detector	L [km]	FV [kton]	$\bar{\rho}$ [g/cm^3]	OA [deg.]
SK	295	22.5	2.60 [25]	2.5/3.0
Oki	653	100	2.75 [25]	0.9/– [25]
Kr	1000	100	2.90 [25]	1.0/0.5 [25]

modes as signal events. The CCQE events are identified as events with only one Čerenkov ring from an electron or muon where the visible energy of the ring is required to be larger than 200 MeV. Since the neutrino beam direction at the far detector is understood well in long-baseline experiments, we can reconstruct the incoming neutrino energy for the CCQE events by [39]

$$E_{\rm rec} = \frac{m_p^2 - (m_n - E_n^b)^2 - m_\ell^2/2 + 2(m_n - E_n^b)E_\ell}{2(m_n - E_n^b - E_\ell + p_\ell \cos\theta_\ell)}, \quad (2.8)$$

assuming that target nucleons are at rest. Here E_ℓ, p_ℓ and θ_ℓ are the charged lepton's energy, magnitude of the three-momentum and polar angle about the neutrino beam direction; m_p, m_n and m_l are the mass of a proton, neutron, and charged lepton, respectively, and E_n^b is the neutron binding energy in the target nucleus. For the anti-neutrino events, m_p and m_n should be exchanged and E_n^b should be replaced with the proton binding energy E_p^b in Eq. (2.8). It should be noted that in reality the reconstructed energy may be different from the incoming neutrino energy due to the Fermi motion of target nucleons inside nuclei and finite detector resolutions for lepton momenta and scattering angles.

The numbers of the signal events in the $i_{\rm th}$ energy bin, $E_{\rm rec}^i < E < E_{\rm rec}^{i+1}$, from the $\nu_\alpha \to \nu_\beta$ oscillation mode at the water Čerenkov detector D (=SK, Oki, Kr) via the X-type neutrino–nucleus interaction (X = CCQE, non-CCQE) are calculated as

$$N_D^{i,X}(\nu_\alpha \to \nu_\beta) = \int_{E_{\rm rec}^i}^{E_{\rm rec}^{i+1}} {\rm d}E_{\rm rec} \int_0^\infty {\rm d}E_\nu \, \Phi_{\nu_\alpha}^D(E_\nu) \, P_{\nu_\alpha \to \nu_\beta}(E_\nu, \bar{\rho}^D) \times \sum_{Z=H,O} N_Z \, \hat{\sigma}_{\nu_\beta Z}^X(E_\nu) \, S_{\nu_\beta Z}^X(E_\nu, E_{\rm rec}), \quad (2.9)$$

where $E^i_{\rm rec} = 0.05\ {\rm GeV} \times i$, E_ν is an incoming neutrino energy, $\Phi^D_{\nu_\alpha}$ is the flux of ν_α at the detector D, $P_{\nu_\alpha \to \nu_\beta}$ is the neutrino oscillation probability including the matter effects with the mean matter density $\bar{\rho}^D$, and N_Z is the number of the Z nuclei (hydrogen (H) or oxygen (O)) in the detector. $\hat{\sigma}^X_{\nu_\beta Z}$ is the cross section of the X-type ν_β–Z interaction after imposing a CCQE selection cuts. The smearing function $S^X_{\nu_\beta Z}(E_\nu, E_{\rm rec})$ returns the probability that the energy $E_{\rm rec}$ is reconstructed from an event induced by an incoming neutrino with the energy E_ν, taking into account the Fermi motion of the target nucleons and detector resolutions. The detection efficiency of Čerenkov rings and the electron/muon identification efficiencies will be discussed in Sects. 2.4 and 3.

In order to estimate the cross sections of the CCQE signal, $\hat{\sigma}^X_{\nu_\beta Z}$, we generate events induced by the neutrino and anti-neutrino charged-current interactions with the Monte-Carlo event generator `Nuance v3.504` [40], imposing the CCQE selection criteria:

$$\begin{aligned}
&\text{Only one charged lepton } (\ell = \mu^\pm \text{ or } e^\pm) \\
&\quad \text{with } |p_\ell| > 200\ {\rm MeV}, && \text{(2.10a)}\\
&\text{No high energy } \pi^\pm\ (|p_{\pi^\pm}| > 200\ {\rm MeV}), && \text{(2.10b)}\\
&\text{No high energy } \gamma\ (|p_\gamma| > 30\ {\rm MeV}), && \text{(2.10c)}\\
&\text{No } \pi^0,\ K_S,\ K_L \text{ and } K^\pm. && \text{(2.10d)}
\end{aligned}$$

The lower limit of the lepton momentum in the first criterion, (2.10a), is from the threshold of the water Čerenkov detector for muons. $\pi^\pm$ with $|p| > 200$ MeV and γ with $|p| > 30$ MeV as well as π^0, K_S, K_L and $K^\pm$ (which are assumed to decay inside a detector) give rise to additional rings. Events with such additional rings are not selected as the CCQE events and are removed. The surviving events after imposing the selection cuts consist of the genuine CCQE events and the other charged-current events (non-CCQE events). Some of the non-CCQE events arise from single soft $\pi^\pm$ emission via the Δ resonance [22]. We parameterize the CCQE and non-CCQE cross sections for target nuclei after imposing the selection criteria (2.10) and summarize them in Appendix A.

The smearing effects due to the Fermi motion and detector resolution shown in Table 2 are taken into account by smearing functions. We made fitting formulas of the anti-neutrino smearing functions for numerical simulations and show them in Fig. 2 for incoming anti-neutrino energy of 1 and 2 GeV. The explicit expressions of the anti-neutrino smearing functions are found in Appendix B. Those for neutrinos are in Ref. [22]. The red circles show simulated distributions for genuine CCQE interactions, while the red histograms show the distributions based on the fitting formulas. The blue diamonds and histograms are for non-CCQE interactions. We see that the fitting formulas describe the simulated distributions well. Anti-neutrinos can interact with protons in hydrogen, in addition to oxygen. Thus, the reconstructed energy distributions show sharper peaks than those for neutrinos since protons in hydrogens do not have the Fermi motion and are almost at rest for anti-neutrinos with $\mathcal{O}(1)$ GeV energy. (The smearing functions for neutrinos are shown in Fig. 3 in Ref. [22].)

Table 2 The momentum and angular resolutions for muons and electrons at the SK detector [41]

	$\delta p/p$ (%)	$\delta\theta$ (°)
μ	$1.7 + 0.7/\sqrt{p[{\rm GeV}]}$	1.8°
e	$0.6 + 2.6/\sqrt{p[{\rm GeV}]}$	3.0°

2.4 Background events

In this section we discuss the sources of background events taken into account in this study: neutral-current (NC) single-π^0 events, secondary neutrinos in the ν_μ and $\bar{\nu}_\mu$ focusing beams and misidentified muon and electron events.

NC single-π^0 events can be a substantial background source for the ν_e and $\bar{\nu}_e$ appearance modes, where one of the photons from a π^0 decay is lost, or the produced π^0 is so energetic that it decays to unresolved photons, mimicking an electron ring. NC neutrino–nucleus scatterings occurs through the quasi-elastic (NCQE), resonant π^0 production (NCRes), coherent π^0 production (NCCoh) or deep-inelastic (NCDI) scatterings. The numbers of the NC single-π^0 events in the $i_{\rm th}$ energy bin, $E^i_{\rm rec} < E < E^{i+1}_{\rm rec}$, at the water Čerenkov detector D (=SK, Oki, Kr) via the Y-type neutrino–nucleus interaction (Y = NCQE, NCRes, NCCoh and NCDI) induced by the ν_α component of the ν_μ or $\bar{\nu}_\mu$ focusing beam are calculated as

$$N^{i,Y}_{\pi^0,D}(\nu_\alpha) = \int_{E^i_{\rm rec}}^{E^{i+1}_{\rm rec}} {\rm d}E_{\rm rec} \int_0^\infty {\rm d}E_\nu\ \Phi^D_{\nu_\alpha}(E_\nu) \times \sum_{Z=H,O} N_Z\, \hat{\sigma}^Y_Z(E_\nu)\, S^Y_Z(E_\nu, E_{\rm rec}), \qquad (2.11)$$

where $E^i_{\rm rec} = 0.05\,{\rm GeV} \times i$, and $\hat{\sigma}^Y_Z$ and S^Y_Z are the cross section and smearing function for the Y-type ν–Z interaction after imposing the NC single-π^0 selection criteria:

$$\begin{aligned}
&\text{No charged leptons}, && \text{(2.12a)}\\
&\text{Only one } \pi^0, && \text{(2.12b)}\\
&\text{No high energy } \pi^\pm\ (|p_{\pi^\pm}| > 200\ {\rm MeV}), && \text{(2.12c)}\\
&\text{No high energy } \gamma\ (|p_\gamma| > 30\ {\rm MeV}), && \text{(2.12d)}\\
&\text{No } K_S,\ K_L \text{ and } K^\pm. && \text{(2.12e)}
\end{aligned}$$

The first condition, Eq. (2.12a), selects NC events, while the other conditions eliminate multi-ring events. The π^0 momentum distributions from the ν_μ focusing beams after imposing

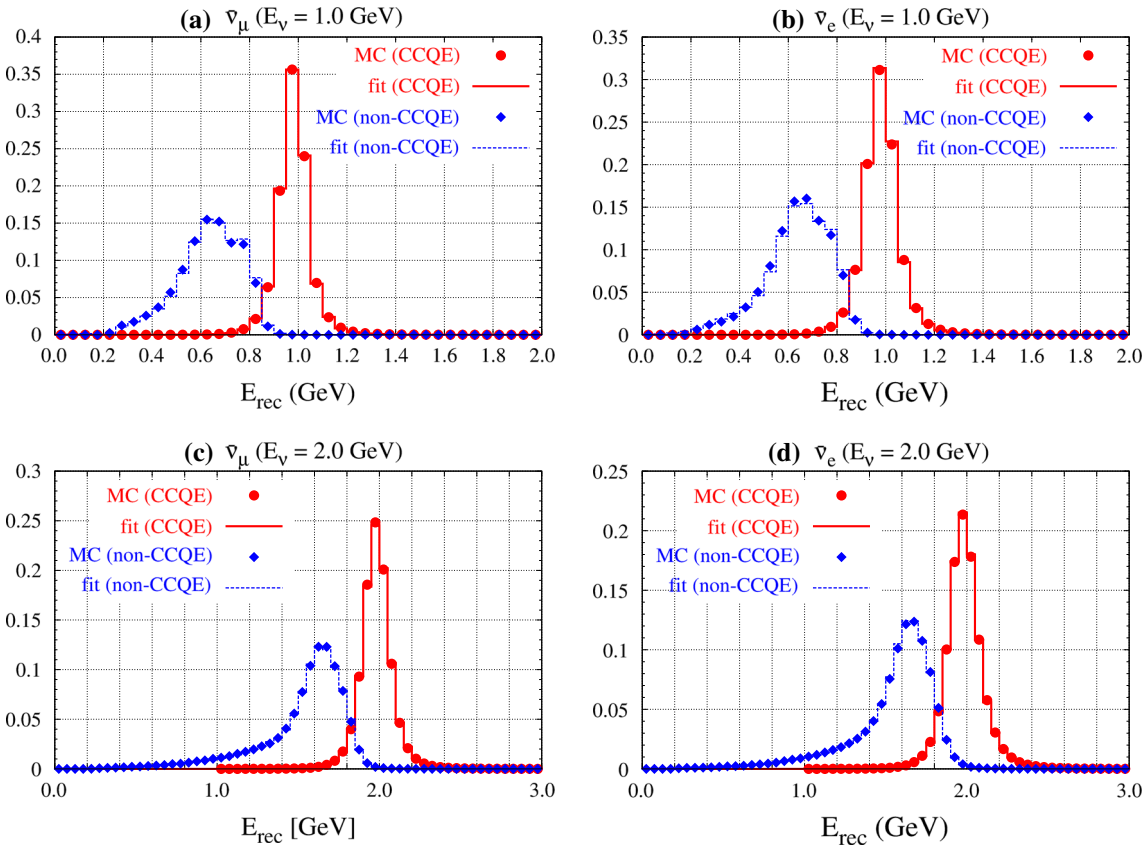

Fig. 2 The normalized reconstructed energy distributions of CCQE (*solid circles*) and non-CCQE (*solid diamonds*) events initiated by monochromatic anti-neutrinos: **a** $\bar{\nu}_\mu$ and **b** $\bar{\nu}_e$ with $E_\nu = 1$ GeV; **c** $\bar{\nu}_\mu$ and **d** $\bar{\nu}_e$ with $E_\nu = 2$ GeV. Those events are generated by `Nuance` `v3.504` [40], imposing the CCQE selection cuts (2.10) and applying the detector resolutions in Table 2 to the produced muons and electrons. The *solid-red* and *dotted-blue* histograms show the fitting formulas of the CCQE and non-CCQE smearing functions, respectively

the above criteria are shown in Fig. 3 for various off-axis beam angles. The NC single-π^0 events are produced more with smaller off-axis beam angle because the fluxes of such neutrino beams are distributed in a higher energy region as shown in Fig. 1. This is a disadvantage of using neutrino beams with smaller off-axis angles at a far detector, and a low π^0 misidentification probability is needed especially for the CP phase measurements. We parameterize the π^0 misidentification probability, P_{e/π^0}, used in our analysis as a function of π^0 momentum x [GeV], as

$$P_{e/\pi^0}(x) = ax(x+b), \tag{2.13}$$

$$a = 0.222\ [1/\mathrm{GeV}^2],$$

$$b = 0.802\ [\mathrm{GeV}], \tag{2.14}$$

based on the simulation [42] of the POLfit π^0-rejection algorithm[2] [31]. The reference data and the fitted function are shown in Fig. 3b. The misidentification probability is kept less than 0.2 for $p_{\pi^0} < 0.6$ GeV, where the π^0 backgrounds mostly distributes. The background events are then selected from the simulated NC single-π^0 events according to the misidentification probability, and the reconstructed energy of each background event is calculated with Eq. (2.8), assuming the misidentified π^0 to be an electron.

The NC single-π^0 backgrounds significantly affect the sensitivity to the mass hierarchy and CP phase [22], and it is important to include their uncertainty properly in our analyses. One of the major uncertainty sources of the NC single-π^0 backgrounds is modeling of neutrino–nucleus interactions. In Fig. 4 we show the reconstructed energy distributions of the NC single-π^0 backgrounds calculated with `Nuance` for different neutrino–nucleus interactions. We see that the π^0 backgrounds mainly distribute in low-energy region, where the contributions from resonant and coherent single-π^0 production processes dominate. These processes are implemented in `Nuance` based on the Rein–Sehgal calculations [32,33]. Among the modeling parameters of the NC neutrino–nucleus interactions, axial form-factor masses

[2] Recently, more efficient π^0 rejection algorithm has been developed by the T2K collaboration [43], and our NC π^0 background estimation may be regarded as a conservative one.

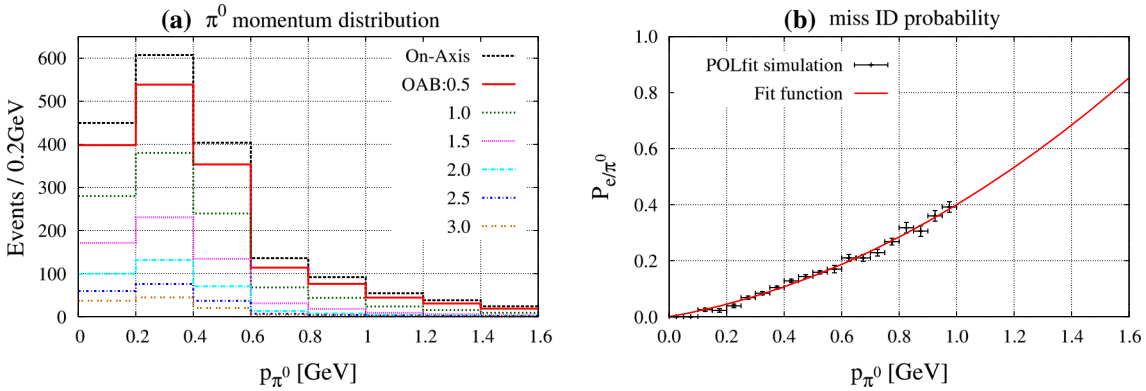

Fig. 3 **a** The π^0 momentum distributions of NC single-π^0 events selected by the criteria (2.12) for various off-axis angles at a far detector. The event numbers are obtained with a 100 kton water target at 1000 km away from the J-PARC and the ν_μ focusing beam flux corresponding to 5×10^{21} POT with the proton energy of 40 GeV. **b** The probability of misidentifying a π^0 to an $e^\pm$ as a function of π^0 momentum, based on the POLfit algorithm [31]. The *black points* show simulated data by the T2K collaboration [42], and the *red curve* show the fitted function to the data, Eq. (2.13)

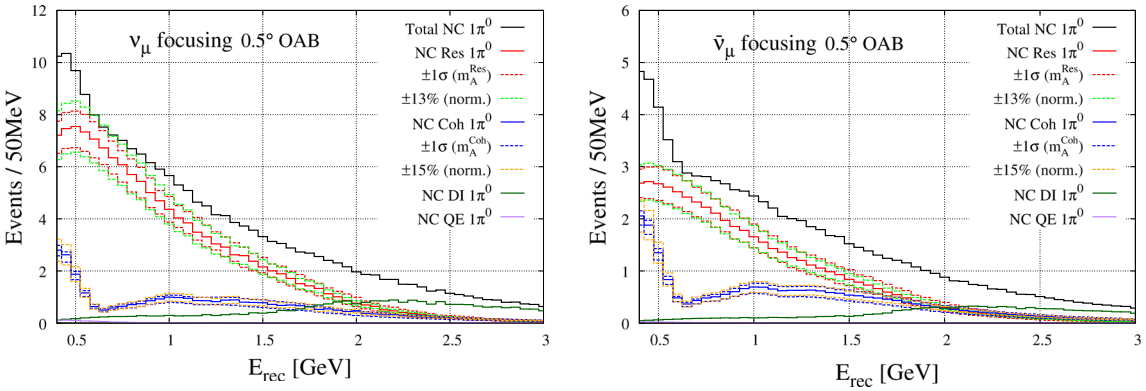

Fig. 4 The reconstructed energy distributions of the NC single-π^0 backgrounds for the ν_μ (*left*) and $\bar{\nu}_\mu$ (*right*) focusing beams. The *solid-red* and *solid-blue histograms* show the NC resonant and coherent single-π^0 components calculated with the axial masses ($m_A^{\rm Res}$ and $m_A^{\rm Coh}$) of 1.1 and 1.03 GeV, respectively. The *dashed-red* and *dashed-blue histograms* show the 1σ uncertainty ranges of the resonant and coherent axial masses, respectively. The *solid-green* and *purple histograms* show the NC deep-inelastic (DI) and quasi-elastic (QE) single-π^0 components, and the *black histogram* is for the total NC single-π^0 backgrounds. Event numbers are calculated for a 100 kton detector using the 0.5° off-axis beam with the ν_μ ($\bar{\nu}_\mu$) flux corresponding to 5×10^{21} POT with the proton energy of 40 GeV

(m_A) have not been measured accurately. Therefore, we vary the axial masses of the resonant and coherent single-pion production processes within their uncertainties: $m_A^{\rm Res} = 1.1 \pm 0.11$ GeV [44] and $m_A^{\rm Coh} = 1.03 \pm 0.28$ GeV [45]. As shown in Fig. 4, those uncertainties can be well approximated by 13 and 15% normalization uncertainties for the NC resonant and coherent single-π^0 backgrounds, respectively.

Another major source of uncertainty of the NC single-π^0 backgrounds arises from the π^0 misidentification probability, Eq. (2.13). The T2K collaboration estimated 10.8% uncertainty in the NC-π^0 background estimation due to the POLfit algorithm [42]. Since our modeling of the π^0 misidentification probability is based on the POLfit algorithm, we assign 11% uncertainty to the normalization of the NC single-π^0 backgrounds due to the π^0 misidentification.

All in all, we include the 13 and 15% normalization uncertainties for the NC resonant and coherent single-π^0 backgrounds, respectively, and 11% normalization uncertainty for the total NC single-π^0 backgrounds. This treatment allows independent normalization corrections for the resonant and coherent NC single-π^0 backgrounds.

The ν_μ ($\bar{\nu}_\mu$) focusing beams contain not only ν_μ ($\bar{\nu}_\mu$) but also other neutrino flavors, ν_e, $\bar{\nu}_e$ and $\bar{\nu}_\mu$ (ν_μ), secondary neutrino beams. Especially, for the $\nu_\mu \to \nu_e$ and $\bar{\nu}_\mu \to \bar{\nu}_e$ oscillation modes, the ν_e and $\bar{\nu}_e$ secondary beams become major background sources. We simulate these secondary-neutrino events in the same way as the signal events described in Sect. 2.3.

There is also some probability of misidentifying a muon (electron) Čerenkov ring as an electron (muon), $P_{e/\mu}$ ($P_{\mu/e}$).

Although these probabilities depend on the detector design and performance, we assume the same probabilities for the SK and the far detector in Oki and Korea as

$$P_{e/\mu} = P_{\mu/e} = 1 \pm 1\%. \tag{2.15}$$

3 χ^2 Analysis

Using the simulated signal and background events, we estimate the sensitivity of the T2KK and T2KO experiments to the mass hierarchy and CP phase ($\delta_{\rm CP}$), performing the χ^2 analysis. The χ^2 function used in this study can be written as

$$\chi^2 \equiv \chi^2_{\rm SK} + \chi^2_{\rm Oki/Kr} + \chi^2_{\rm sys} + \chi^2_{\rm para}. \tag{3.1}$$

The first two terms measure deviations of data from the theoretical predictions at the SK and a far detector in Oki or Korea,

$$\begin{aligned}\chi^2_D = \sum_i \Bigg\{ &\left(\frac{(N^i_{\mu,D})^{\rm fit} - (N^i_{\mu,D})^{\rm input}}{\sqrt{(N^i_{\mu,D})^{\rm fit}}} \right)^2 \\ &+ \left(\frac{(\overline{N}^i_{\mu,D})^{\rm fit} - (\overline{N}^i_{\mu,D})^{\rm input}}{\sqrt{(\overline{N}^i_{\mu,D})^{\rm fit}}} \right)^2 \\ &+ \left(\frac{(N^i_{e,D})^{\rm fit} - (N^i_{e,D})^{\rm input}}{\sqrt{(N^i_{e,D})^{\rm fit}}} \right)^2 \\ &+ \left(\frac{(\overline{N}^i_{e,D})^{\rm fit} - (\overline{N}^i_{e,D})^{\rm input}}{\sqrt{(\overline{N}^i_{e,D})^{\rm fit}}} \right)^2 \Bigg\}, \end{aligned} \tag{3.2}$$

where $(N^i_{\mu,D})^{\rm input}$ and $(N^i_{e,D})^{\rm input}$ denote the μ- and e-like event numbers, respectively, in the ith bin of the $E_{\rm rec}$ distributions measured at a detector D (=SK, Oki, Kr) from the ν_μ focusing beam, and $(\overline{N}^i_{\mu,D})^{\rm input}$ and $(\overline{N}^i_{e,D})^{\rm input}$ are those from the $\bar{\nu}_\mu$ focusing beam. The summation runs over all the $E_{\rm rec}$ bins from 0.4 to 5.0 GeV at both the SK and the far (Oki or Kr) detectors.

The μ- and e-like event numbers are calculated using the CC signal and NC single-π^0 background events ($N^{i,X}_D$ and $N^{i,Y}_{\pi^0,D}$ defined by Eqs. (2.9) and (2.11)) as

$$\begin{aligned}(N^i_{\mu,D})^{\rm input} = {} & (1 - P^D_{e/\mu})\varepsilon^D_\mu \sum_{X,\nu_\alpha} \{N^{i,X}_D(\nu_\alpha \to \nu_\mu) \\ & + N^{i,X}_D(\nu_\alpha \to \bar{\nu}_\mu)\} \\ & + P^D_{\mu/e}\, \varepsilon^D_e \sum_{X,\nu_\alpha} \{N^{i,X}_D(\nu_\alpha \to \nu_e) \\ & + N^{i,X}_D(\nu_\alpha \to \bar{\nu}_e)\}, \end{aligned} \tag{3.3a}$$

$$\begin{aligned}(N^i_{e,D})^{\rm input} = {} & P^D_{e/\mu}\, \varepsilon^D_\mu \sum_{X,\nu_\alpha} \{N^{i,X}_D(\nu_\alpha \to \nu_\mu) \\ & + N^{i,X}_D(\nu_\alpha \to \bar{\nu}_\mu)\} \\ & + (1 - P^D_{\mu/e})\, \varepsilon^D_e \sum_{X,\nu_\alpha} \{N^{i,X}_D(\nu_\alpha \to \nu_e) \\ & + N^{i,X}_D(\nu_\alpha \to \bar{\nu}_e)\} + \sum_{Y,\nu_\alpha} N^{i,Y}_{\pi^0,D}(\nu_\alpha), \end{aligned} \tag{3.3b}$$

where ε^D_μ (ε^D_e) is the efficiency of detecting muon (electron) Čerenkov rings, and $P^D_{e/\mu}$ ($P^D_{\mu/e}$) is the probability of misidentifying the detected muon (electron) Čerenkov ring as an electron (muon). Detected neutrino flavors are already summed in $N^{i,Y}_{\pi^0,D}$. The anti-neutrino event numbers $(\overline{N}^i_{\mu,D})^{\rm input}$ and $(\overline{N}^i_{e,D})^{\rm input}$ are calculated with similar expressions as Eqs. (3.3a) and (3.3b). It should be noted that we neglect statistical fluctuations in the input event numbers, and those event numbers should be considered as averaged ones. The reconstructed energy distributions for the μ- and e-like events are shown in Figs. 5, 6 and 7, which are calculated using the input parameter values in Table 3.

As shown in those figures, T2KK and T2KO experiments can observe up to the second peak of the $\nu_\mu \to \nu_e$ and $\bar{\nu}_\mu \to \bar{\nu}_e$ oscillations due to their long-baseline length, while the T2K experiment only observes the first peak. Observing the several peaks of those oscillation modes has advantages especially for the accurate CP phase measurement because tails of the oscillation peaks have the information of both $\sin\delta_{\rm CP}$ and $\cos\delta_{\rm CP}$.

On the other hand, the theoretical predictions of the μ- and e-like event numbers, $(N^i_{\mu,D})^{\rm fit}$ and $(N^i_{e,D})^{\rm fit}$, are calculated as

$$\begin{aligned}(N^i_{\mu,D})^{\rm fit} = f^D_{\rm V} \Bigg[& (1 - P^D_{e/\mu})\varepsilon^D_\mu \sum_{X,\nu_\alpha} f^D_{\nu_\alpha} \{ f^X_{\nu_\mu} N^{i,X}_D(\nu_\alpha \to \nu_\mu) \\ & + f^X_{\bar{\nu}_\mu} N^{i,X}_D(\nu_\alpha \to \bar{\nu}_\mu)\} \\ & + P^D_{\mu/e}\, \varepsilon^D_e \sum_{X,\nu_\alpha} f^D_{\nu_\alpha} \{ f^X_{\nu_e} N^{i,X}_D(\nu_\alpha \to \nu_e) \\ & + f^X_{\bar{\nu}_e} N^{i,X}_D(\nu_\alpha \to \bar{\nu}_e)\} \Bigg], \end{aligned} \tag{3.4a}$$

$$\begin{aligned}(N^i_{e,D})^{\rm fit} = f^D_{\rm V} \Bigg[& P^D_{e/\mu}\, \varepsilon^D_\mu \sum_{X,\nu_\alpha} f^D_{\nu_\alpha} \{ f^X_{\nu_\mu} N^{i,X}_D(\nu_\alpha \to \nu_\mu) \\ & + f^X_{\bar{\nu}_\mu} N^{i,X}_D(\nu_\alpha \to \bar{\nu}_\mu)\} \\ & + (1 - P^D_{\mu/e})\varepsilon^D_e \sum_{X,\nu_\alpha} f^D_{\nu_\alpha} \{ f^X_{\nu_e} N^{i,X}_D(\nu_\alpha \to \nu_e) \\ & + f^X_{\bar{\nu}_e} N^{i,X}_D(\nu_\alpha \to \bar{\nu}_e)\} \Bigg] \end{aligned}$$

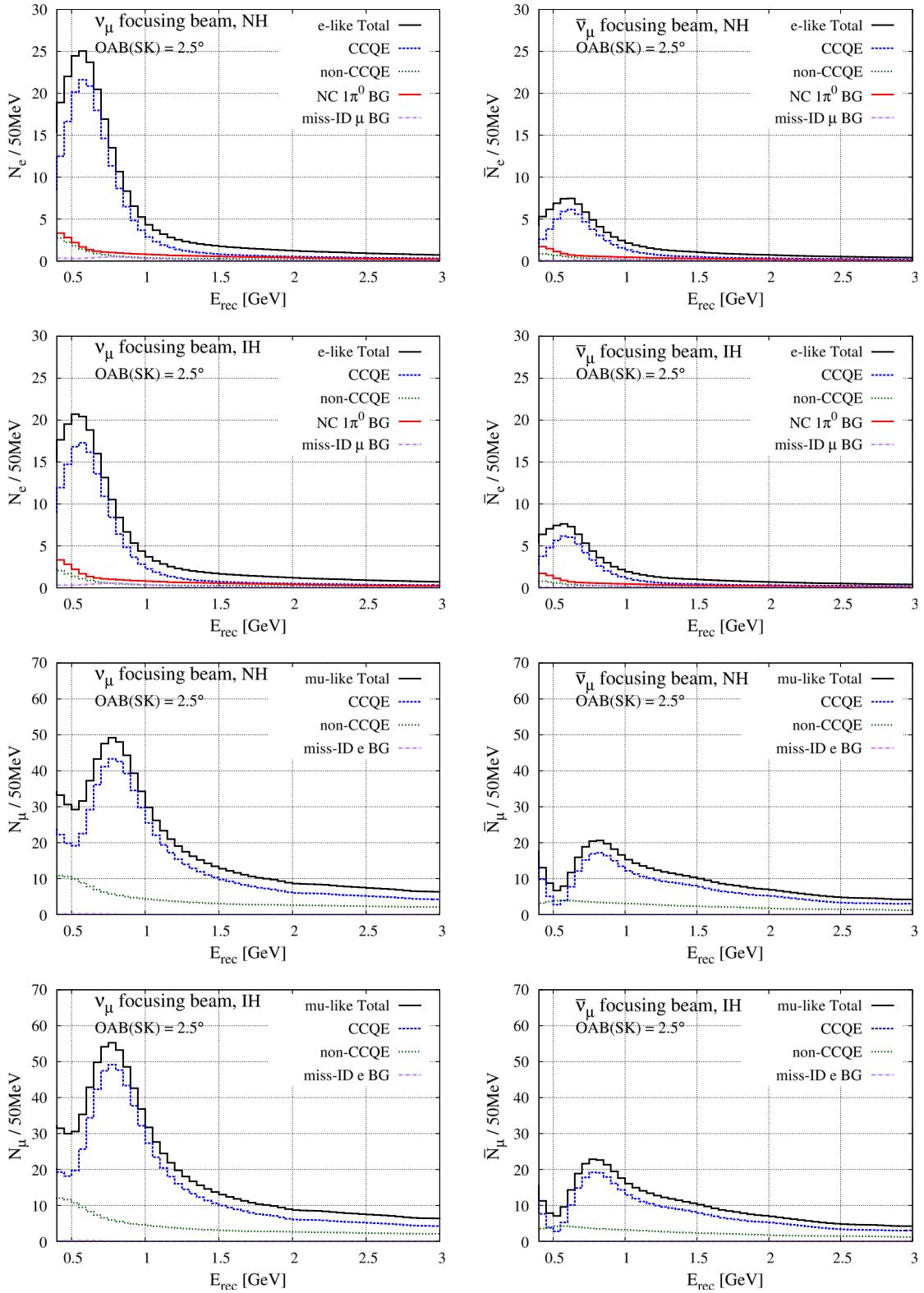

Fig. 5 The reconstructed energy distributions at the SK detector with the ν_μ (*left panels*) and $\bar{\nu}_\mu$ (*right panels*) focusing beams. The former four panels show distributions for *e*-like events, and the latter four panels are for μ-like events. The first and third rows are for the normal hierarchy case, while the second and fourth rows are for the inverted hierarchy case. The *dashed-blue*, *dotted-green*, *red* and *dash-dotted-purple* *histograms* are for CCQE, non-CCQE, NC single-π^0 background and misidentified muon/electron background events, respectively. The *black histogram* shows the total of those contributions. The event numbers are calculated for the T2K experiment with the 2.5° OAB and the beam flux corresponding to 5×10^{21} POT with the proton energy of 40 GeV

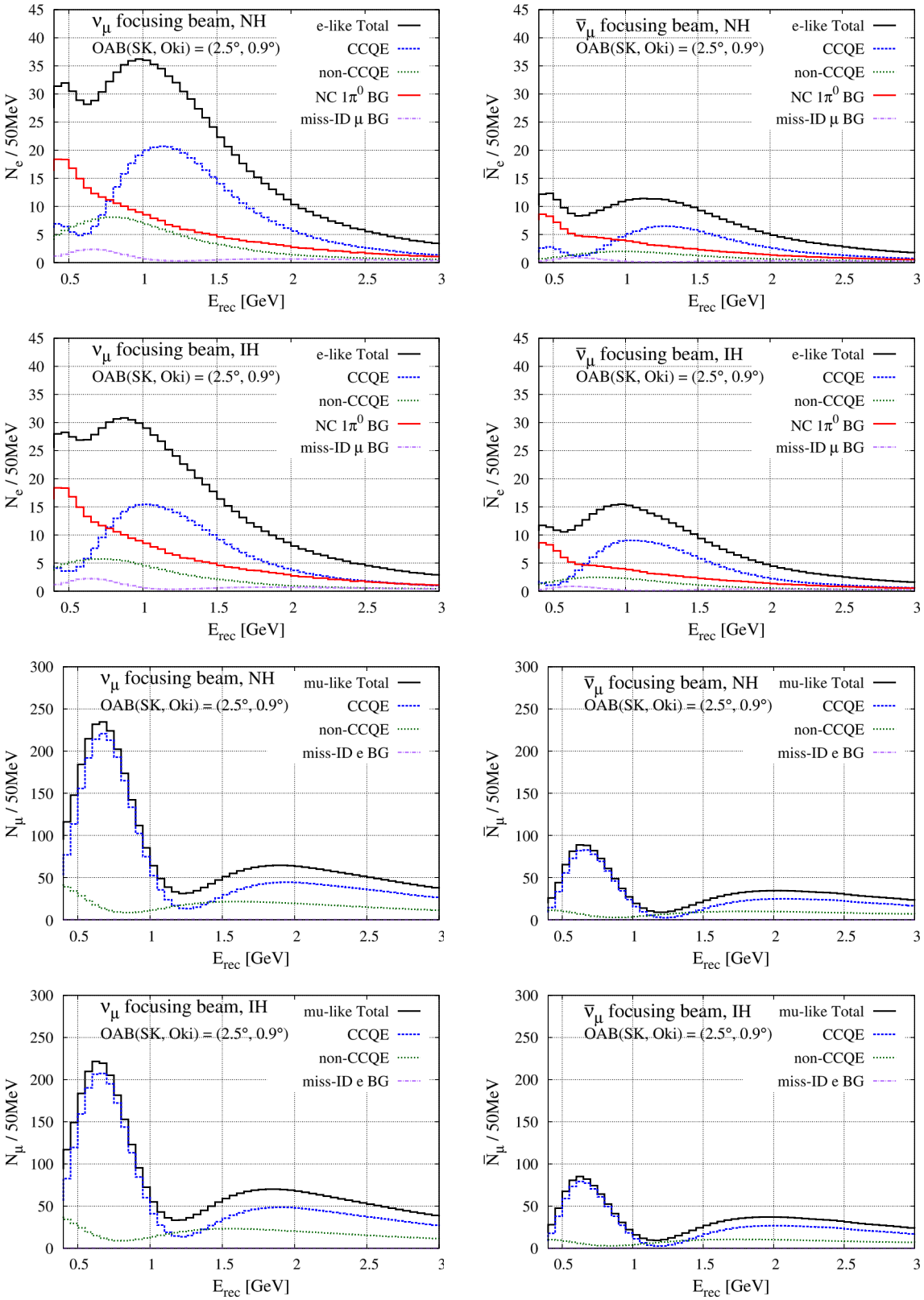

Fig. 6 Same as Fig. 5 but for the T2KO experiment with the 0.9° OAB at an Oki detector with the 100 kton fiducial volume

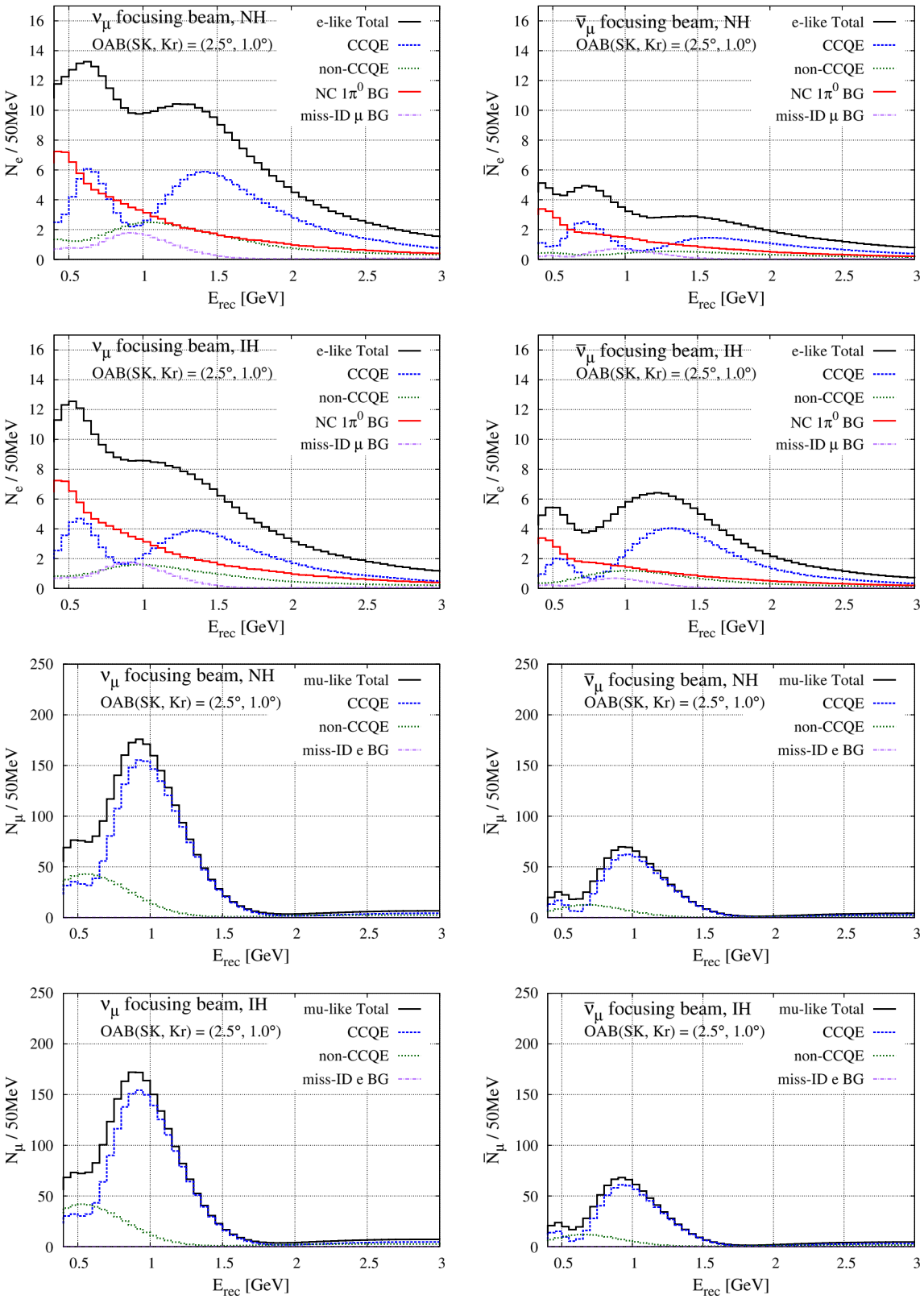

Fig. 7 Same as Fig. 5 but for the T2KK experiment with the 1.0° OAB at a Kr detector with the 100 kton fiducial volume

Table 3 The systematic and physical parameters in the χ^2 function, Eq. (3.1), where D stands for the detector site (SK, Oki and Kr), and ν_α or ν_β denotes neutrino species (ν_μ, $\bar{\nu}_\mu$, ν_e and $\bar{\nu}_e$). These input values and uncertainties are used in the sensitivity study otherwise mentioned

Systematic parameters (S)	Input value ($S_{\rm input}$)	Uncertainty (δS)
Fiducial volume of detectors (f_V^D)	1.00	0.03 [22]
Neutrino flux at a detector ($f_{\nu_\alpha}^D$)	1.00	0.03 [22]
CCQE cross sections ($f_{\nu_\beta}^{\rm CCQE}$)	1.00	0.03 [22]
Non-CCQE cross sections ($f_{\nu_\beta}^{\rm nonCCQE}$)	1.00	0.20 [22]
Misidentified NC π^0 events ($f_{\pi^0}^{\rm NC}$)	1.00	0.11
Misidentified NC resonant π^0 events ($f_{\pi^0}^{\rm NCRes}$)	1.00	0.13
Misidentified NC coherent π^0 events ($f_{\pi^0}^{\rm NCCoh}$)	1.00	0.15
Detection efficiency of electron Čerenkov rings (ϵ_e^D)	0.90	0.05 [22]
Detection efficiency of muon Čerenkov rings (ϵ_μ^D)	1.00	0.01 [22]
μ-to-e miss-ID probability ($P_{e/\mu}^D$)	0.01	0.01 [22]
e-to-μ miss-ID probability ($P_{\mu/e}^D$)	0.01	0.01 [22]

Physical parameters (P)	Input value ($P_{\rm input}$)	Uncertainty (δP)
$\sin^2 2\theta_{12}$	0.875	0.024 [34]
$\sin^2 2\theta_{13}$	0.095 [34]	0.005 [46]
$\sin^2 \theta_{23}$	0.5	0.1 [34]
δm^2_{21} [eV]^2	7.50×10^{-5}	0.20×10^{-5} [34]
$\lvert\delta m^2_{32}\rvert$ [eV]^2	2.32×10^{-3}	0.10×10^{-3} [34]
$\delta_{\rm CP}$	0°	–
$\bar{\rho}^{\rm SK}$ [g/cm^3]	2.60	6% [25]
$\bar{\rho}^{\rm Oki}$ [g/cm^3]	2.75	6% [25]
$\bar{\rho}^{\rm Kr}$ [g/cm^3]	2.9	6% [25]

$$+ f_{\rm V}^D \sum_{\nu_\alpha} f_{\nu_\alpha}^D f_{\pi^0}^{\rm NC} \{ f_{\pi^0}^{\rm NCRes} N_{\pi^0,D}^{i,\rm NCRes}(\nu_\alpha) + f_{\pi^0}^{\rm NCCoh} N_{\pi^0,D}^{i,\rm NCCoh}(\nu_\alpha) + N_{\pi^0,D}^{i,\rm NCDI}(\nu_\alpha) + N_{\pi^0,D}^{i,\rm NCQE}(\nu_\alpha) \}, \quad (3.4b)$$

where f_V^D and $f_{\nu_\alpha}^D$ are the normalization factors for the fiducial volume of and the ν_α flux at a detector D (=SK, Oki, Kr), respectively. $f_{\nu_\beta}^X$ is the normalization factor for the CC cross section of a neutrino flavor ν_β via a X(=CCQE or non-CCQE) interaction. $f_{\pi^0}^{\rm NCRes}$ and $f_{\pi^0}^{\rm NCCoh}$ are the normalization factors for the NC cross sections of resonant and coherent single-π^0 production processes, respectively, while $f_{\pi^0}^{\rm NC}$ is the overall normalization factor for the NC single-π^0 backgrounds, mainly reflecting the uncertainty of the π^0 misidentification probability, Eq. (2.13). These factors are varied in the minimization of the χ^2 function, and their deviation from unity measures systematic uncertainties.

Using the above normalization factors, detection efficiencies ($\varepsilon_e, \varepsilon_\mu$) and misidentification probabilities ($P_{e/\mu}, P_{\mu/e}$), we take into account the effects of the systematic uncertainty in the χ^2 function as

$$\chi^2_{\rm sys} = \sum_S \left(\frac{S_{\rm fit} - S_{\rm input}}{\delta S} \right)^2, \quad (3.5)$$

where $S_{\rm fit}$ is the systematic parameter value used to calculate the theoretical predictions, $S_{\rm input}$ is the one used to generate the data, and δS is the uncertainty of the parameter. We summarize the systematic parameters used in our analysis in Table 3, where the uncertainties related to the NC π^0 backgrounds are assigned based on the discussions in Sect. 2.4, while the other uncertainties are taken as in the previous study [22].

Finally, $\chi^2_{\rm para}$ accounts for external constraints on the physical parameters as

$$\chi^2_{\rm para} = \sum_P \left(\frac{P_{\rm fit} - P_{\rm input}}{\delta P} \right)^2, \quad (3.6)$$

where $P_{\rm fit}$ is the parameter value used to calculate the theoretical predictions, $P_{\rm input}$ is the one used to generate the data, and δP is the uncertainty of the parameter. We summarize the physical parameters used in our analysis in Table 3 as well, where the parameter values are based on Ref. [34], except the uncertainty of $\sin^2 2\theta_{13}$, for which we use the uncertainty achieved by DayaBay collaboration [46], and the matter densities, which are taken from the Refs. [24,25].

The sensitivities to the mass hierarchy are then estimated using the test statistic defined as

$$\Delta\chi^2_{\rm MH} = \chi^2_{\rm min}|_{\rm IH} - \chi^2_{\rm min}|_{\rm NH}, \quad (3.7)$$

where $\chi^2_{\rm min}|_{\rm NH(IH)}$ is the minimum of the χ^2 function under the assumption of the normal (inverted) hierarchy. The distribution of the $\Delta\chi^2_{\rm MH}$ due to the fluctuation of data can be approximated as [47–49]

$$\Delta\chi^2_{\rm MH} \sim \mathcal{N}\left(\overline{\Delta\chi^2_{\rm MH}},\ 2\sqrt{|\overline{\Delta\chi^2_{\rm MH}}|}\right), \tag{3.8}$$

where $\mathcal{N}(\mu,\sigma)$ denotes the normal distribution with mean μ and standard deviation σ; $\overline{\Delta\chi^2_{\rm MH}}$ is the $\Delta\chi^2_{\rm MH}$ obtained with the average experiment (the Asimov data set [50]). It has been shown with explicit Monte Carlo studies that this approximation holds with good accuracy for long-baseline experiments which give $|\overline{\Delta\chi^2_{\rm MH}}| \gg 1$ [49]. With this approximation, we may calculate the probability that an experiment rejects the wrong mass hierarchy hypothesis with a given confidence level. For example, ∼50% is the probability for an experiment to reject the wrong mass hierarchy with the $\sqrt{|\overline{\Delta\chi^2_{\rm MH}}|}$-$\sigma$ confidence level.

The sensitivity to the CP phase measurement is estimated in terms of $(\Delta\chi^2)_{\rm min}$ defined as

$$(\Delta\chi^2)_{\rm min}(\theta) = \min_{\theta'}\chi^2(\theta,\theta')|_{\rm trueMH} - \min_{\theta,\theta'}\chi^2(\theta,\theta')|_{\rm trueMH}, \tag{3.9}$$

where the minimum of the χ^2 function in the first term is found by fixing some model parameters θ and marginalizing the other parameters θ', assuming that the true mass hierarchy is known, while the minimum of the χ^2 function in the second term is found by marginalizing the whole parameters, θ and θ'. Under certain conditions (especially linear dependence of the theoretical prediction on the parameters θ), the $(\Delta\chi^2)_{\rm min}(\theta_{\rm true})$ is known to be approximately distributed as the χ^2 distribution of N_θ degrees of freedom (d.o.f) when the data size is large, where $\theta_{\rm true}$ is the true values of the parameters θ, and N_θ is the number of the fixed parameters [51].

Since the CP phase is a cyclic parameter in the oscillation probabilities, the linearity condition is not satisfied in general, and deviation of the distribution of $(\Delta\chi^2)_{\rm min}(\delta_{\rm CP_{true}})$ form the χ^2 distribution of 1 d.o.f would be expected [52,53]. However, this deviation is not so significant for experiments with sufficiently high sensitivity such that the 1-σ uncertainty of $\delta_{\rm CP}$ measurement is less than ∼20° for $\delta_{\rm CP} = 0°$ [52]. This is the case for the T2KK and T2KO experiments as we will see later, and we estimate the sensitivity to the CP phase of those experiments based on the χ^2 distribution approximation of the $(\Delta\chi^2)_{\rm min}(\delta_{\rm CP_{true}})$ distribution.[3] The n-σ confidence interval of the CP phase measurement, $[\delta^a_{\rm CP}, \delta^b_{\rm CP}]_{n\sigma}$ $(\delta^a_{\rm CP} < \delta^b_{\rm CP})$, is then estimated such that

$$(\Delta\chi^2)_{\rm min}(\delta^a_{\rm CP}) = (\Delta\chi^2)_{\rm min}(\delta^b_{\rm CP}) = n^2 \Longleftrightarrow [\delta^a_{\rm CP}, \delta^b_{\rm CP}]_{n\sigma}. \tag{3.10}$$

[3] In this approximation, the resultant sensitivities would be slightly overestimated, as discussed in Ref. [52].

4 Sensitivity to the mass-hierarchy determination

In this section, we present the results for the sensitivity studies on the mass-hierarchy determination by the T2KK and T2KO experiments, discussing the sensitivity dependence on the ν_μ–$\bar{\nu}_\mu$ focusing beam ratio and $\sin^2\theta_{23}$.

In Fig. 8, the sensitivity of the T2KK experiments to the mass-hierarchy determination is shown. The left and right panels are for the normal and inverted hierarchy cases, while the upper and lower panels are for the 3.0° (0.5°) and 2.5° (1.0°) off-axis beams, OAB, at the SK (Kr) detector, respectively. The true value of $\sin^2\theta_{23}$ is assumed to be 0.5. The blue (dashed-blue), green (dashed-green), orange (dashed-orange) and red curves show the absolute value of the $\overline{\Delta\chi^2_{\rm MH}}$, Eq. (3.8), for rejecting the wrong mass hierarchy when the ratio of the ν_μ and $\bar{\nu}_\mu$ focusing beams is 5:0 (0:5), 4:1 (1:4), 3:2 (2:3) and 2.5:2.5 ($\times 10^{21}$ POT with the proton energy of 40 GeV), respectively. It is shown that including $\bar{\nu}_\mu$ focusing beam can improve the sensitivity, especially in high sensitivity regions. Although inclusion of the $\bar{\nu}_\mu$ focusing beam causes the reduction of sensitivities for some $\delta_{\rm CP}$, this can be alleviated by adjusting the beam ratio appropriately.

In order to minimize the reduction of the sensitivities, $\nu_\mu : \bar{\nu}_\mu = 4{:}1$ is the best ratio for both OAB cases. Comparing the lowest $|\overline{\Delta\chi^2_{\rm MH}}|$ in the whole range of the CP phase, $\nu_\mu : \bar{\nu}_\mu = 4{:}1$ is the best ratio for the 3.0° OAB at the SK, and 3:2–2:3 are the best for the 2.5° OAB at the SK. In terms of the highest sensitivity, 4:1, 3:2, and 2.5:2.5 beam ratios give comparable sensitivity for the normal hierarchy, but 3:2–2.5:2.5 are significantly better than 4:1 for the inverted hierarchy case. Thus, around 3:2–2.5:2.5 would be a preferred choice for 3.0° OAB at the SK. For the 2.5° OAB at the SK, the beam ratio of 3:2–2.5:2.5 would be a preferred choice. Although there is not such a ν_μ–$\bar{\nu}_\mu$ focusing beam ratio that gives the best sensitivity for any $\delta_{\rm CP}$ values and mass hierarchies, the beam ratio between 4:1 and 2.5:2.5 would be a reasonable choice for both 2.5° and 3.0° OAB at the SK.

In Fig. 9, we show the sensitivities of the T2KO experiment. Improvement of the sensitivities by including the $\bar{\nu}_\mu$ focusing beam is significant in the high sensitivity region, preferring the running ratio of 3:2–2:3, while improvement in the low sensitivity region is not so evident. Comparing to the T2KK experiments, the sensitivity is lower by 20–80% in $|\overline{\Delta\chi^2_{\rm MH}}|$. The lower sensitivity in the T2KO experiment is basically due to the smaller matter effects. The difference between the mass hierarchies mainly shows up in A^e and B^e

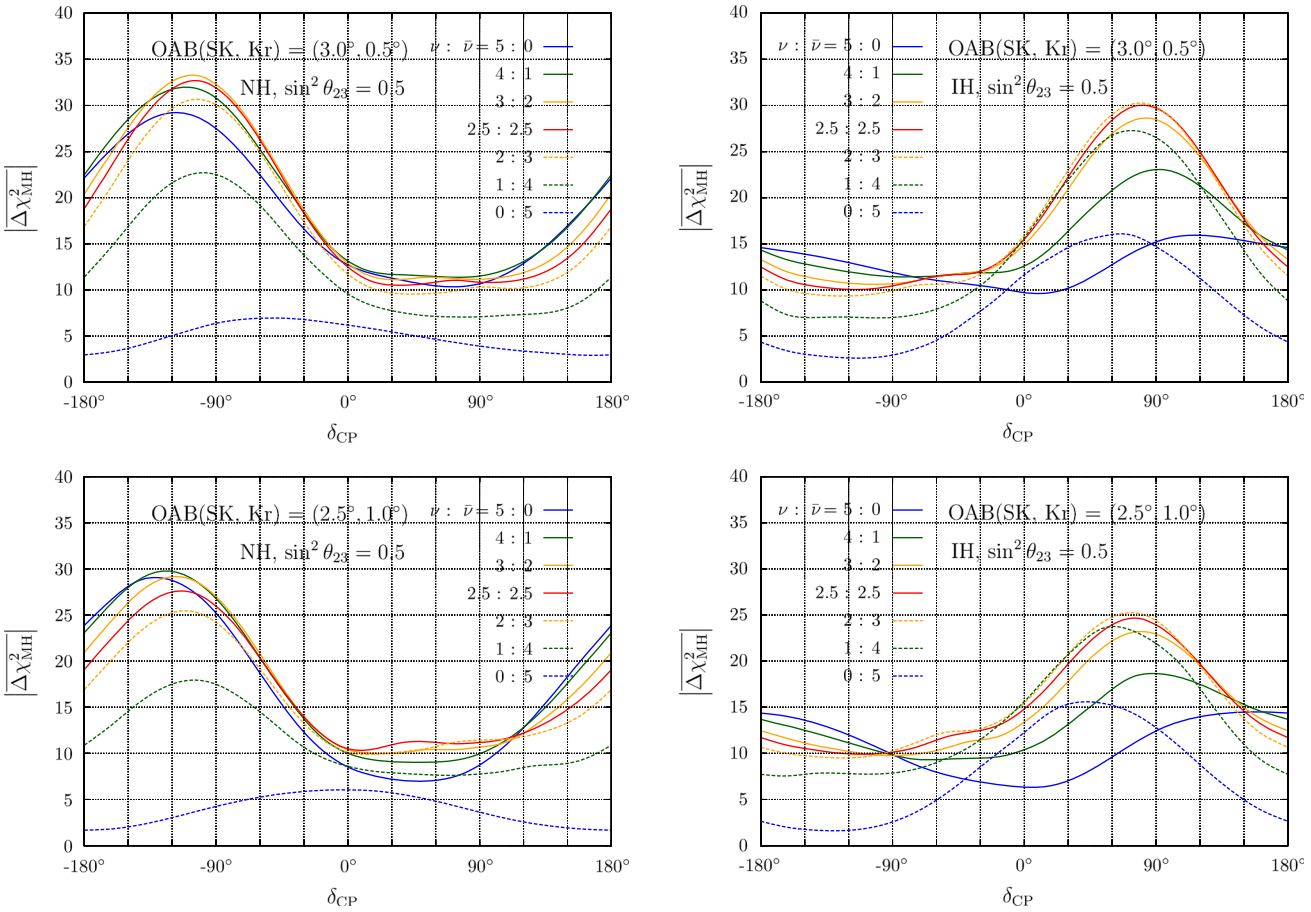

Fig. 8 The $|\overline{\Delta\chi^2_{\rm MH}}|$ for the T2KK experiment to reject the wrong mass hierarchy as a function of the CP phase, $\delta_{\rm CP}$, with $\sin^2\theta_{23} = 0.5$. The *left* and *right panels* are for the normal and inverted hierarchy cases, while the *upper* and *lower panels* are for the 3.0° (0.5°) and 2.5° (1.0°) off-axis beams at the SK (Kr) detector, respectively. The *blue* (*dashed-blue*), *green* (*dashed-green*), *orange* (*dashed-orange*) and *red curves* show the sensitivities when the ν_μ–$\bar{\nu}_\mu$ focusing beam ratio is 5:0 (0:5), 4:1 (1:4), 3:2 (2:3) and 2.5:2.5 $\times 10^{21}$ POT, respectively, with the proton energy of 40 GeV

in Eq. (2.6b) through the matter effects, and is enhanced by the baseline length. Because of the shorter baseline length to the Oki detector than the detector in Korea, this enhancement is reduced more easily by adjusting the CP phase, resulting in the lower sensitivity to the mass hierarchy in the T2KO experiment.

We show the $\sin^2\theta_{23}$ dependence of the sensitivity to the mass-hierarchy determination in Fig. 10. The left and right plots are for the T2KK and the T2KO experiments with the 2.5° OAB at the SK, respectively. The red and dashed-blue curves are for the normal and inverted hierarchy cases. $\sin^2\theta_{23}$ is assumed to be 0.6, 0.5, and 0.4 from the top to the bottom curves for both mass hierarchy cases. We fix the ν_μ–$\bar{\nu}_\mu$ beam ratio at 2.5:2.5, but dependence on $\sin^2\theta_{23}$ are similar in the other beam ratios. The $|\overline{\Delta\chi^2_{\rm MH}}|$ is reduced by up to 30–40% when $\sin^2\theta_{23}$ decreases by 0.1 since the number of the ν_e appearance signal decreases. We will reject the wrong mass hierarchy with $|\overline{\Delta\chi^2_{\rm MH}}| > 8$ (T2KK) and >3 (T2KO) for any CP phases and $\sin^2\theta_{23} > 0.4$. In the most sensitive region around $\delta_{\rm CP} = -90°$ for the normal hierarchy case, we may reject the wrong mass hierarchy with $|\overline{\Delta\chi^2_{\rm MH}}| > 20$ in the T2KK experiment and >14 in the T2KO experiment with $\sin^2\theta_{23} > 0.4$. For the inverted hierarchy case, the most sensitive region is around $\delta_{\rm CP} = 90°$, and we may reject the wrong mass hierarchy with $|\overline{\Delta\chi^2_{\rm MH}}| > 18$ in the T2KK experiment and >14 in the T2KO experiment with $\sin^2\theta_{23} > 0.4$.

5 Sensitivity to the CP phase measurement

In this section, we discuss the sensitivities of the T2KK and T2KO experiments to the CP phase measurement, comparing to an experiment where a 100 kton detector is placed at the Kamioka site in addition to the 22.5 kton SK detector, which is called the $\rm T2K_{122}$ experiment in this study. Comparison

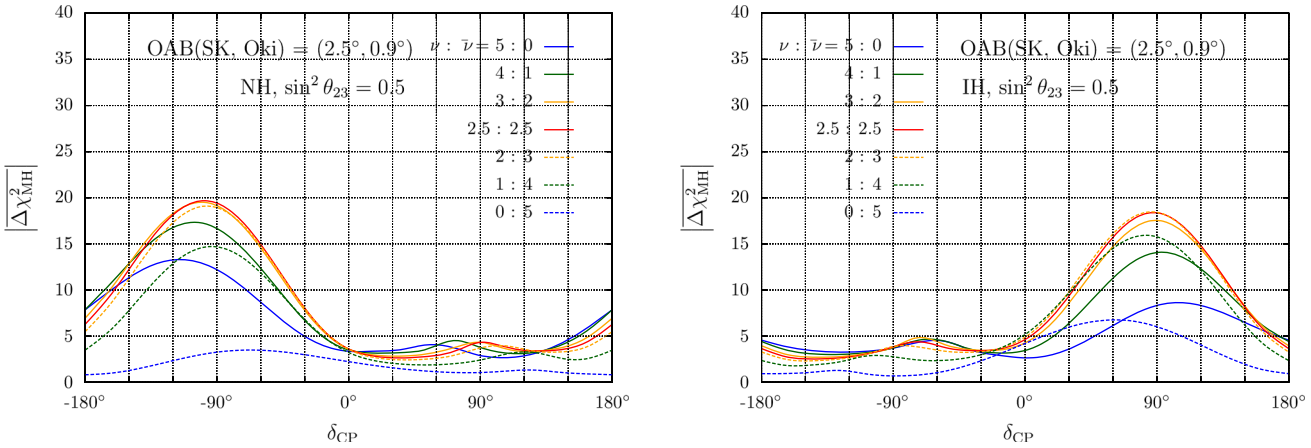

Fig. 9 Same as Fig. 8, but for the T2KO experiment with the 2.5° (0.9°) off-axis beam at the SK (Oki)

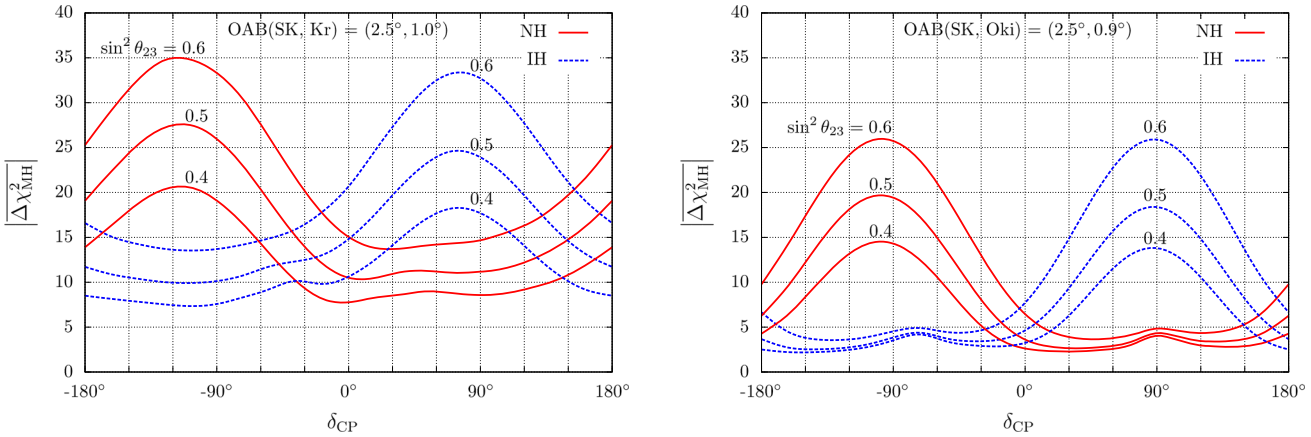

Fig. 10 The dependence of the $|\overline{\Delta\chi^2_{\rm MH}}|$ on $\sin^2\theta_{23}$ for the T2KK and T2KO experiments to reject the wrong mass hierarchy as functions of the CP phase. The *left* and *right* plots are for the T2KK and T2KO experiments with the 2.5° OAB at the SK, respectively. The *red* and *dashed-blue curves* are for the normal and inverted hierarchy cases. $\sin^2\theta_{23}$ is assumed to be 0.6, 0.5, and 0.4 from the *top* to the *bottom curves*. The ν_μ–$\bar{\nu}_\mu$ focusing beam ratio is fixed at $\nu_\mu : \bar{\nu}_\mu = 2.5{:}2.5 \times 10^{21}$ POT with the proton energy of 40 GeV

with this experiment will clearly show the dependence of the CP phase sensitivity on the baseline length. We put emphasis on the effects of including the $\bar{\nu}_\mu$ focusing beam.

In Fig. 11, we show the uncertainties of the CP phase measurements as functions of the true CP phase, $\delta_{\rm CP}^{\rm true}$, for the four experiments: (a) T2KK with 3.0° OAB at the SK and 0.5° OAB at the Kr, (b) T2KK with 2.5° OAB at the SK and 1.0° OAB at the Kr, (c) T2KO and (d) T2K$_{122}$. The uncertainty is defined by the deviation of the test $\delta_{\rm CP}$ from the true $\delta_{\rm CP}$ which gives $(\Delta\chi^2)_{\rm min} = 1$. The curves correspond to the different ν_μ–$\bar{\nu}_\mu$ focusing beam ratios: 4.5:0.5 (*solid-red*), 3.5:1.5 (*solid-blue*), 2.5:2.5 (*solid-green*), 1.5:3.5 (*dashed-blue*) and 0.5:4.5 (*dashed-red*) in units of 10^{21} POT. The uncertainty of the CP phase measurements is smallest around $\delta_{\rm CP} = 0°$ and 180°. This is because the uncertainty mainly reflects the $\sin\delta_{\rm CP}$ dependence of the signal event number since the magnitude of the $\sin\delta_{\rm CP}$ term is larger than that of the $\cos\delta_{\rm CP}$ term in Eq. (2.6b) on average.

On the other hand, the uncertainty is largest around $\delta_{\rm CP} = \pm 60°$ and $\pm 120°$ as clearly shown in the T2K$_{122}$ experiment, Fig. 11d; for the T2KK and T2KO experiments, the low sensitivity regions slightly shift from $\pm 60°$ and $\pm 120°$ due to the matter effects [54]. This low sensitivity reflects the degeneracy between $\delta_{\rm CP}$ and $\pi - \delta_{\rm CP}$ in $\sin\delta_{\rm CP}$. To resolve the degeneracy, we need information of the $\cos\delta_{\rm CP}$ term, which becomes large around tails of oscillation peaks. The T2KK and T2KO experiments observe up to the second peak of the $\nu_\mu \to \nu_e$ and $\bar{\nu}_\mu \to \bar{\nu}_e$ oscillations, while the T2K$_{122}$ experiment only observes the first peak (see Figs. 5, 6, 7). Therefore, the former experiments are more sensitive to the $\cos\delta_{\rm CP}$ term and can measure the CP phase more accurately around those low sensitive regions.

As for the ν_μ–$\bar{\nu}_\mu$ focusing beam ratio, $\nu_\mu{:}\bar{\nu}_\mu = 3.5{:}1.5$–$1.5{:}3.5$ give the smallest uncertainty for most of the CP phases, except for the low sensitivity region, where the ratio of 4.5:0.5 gives the best accuracy. Using the 2.5:2.5 beam

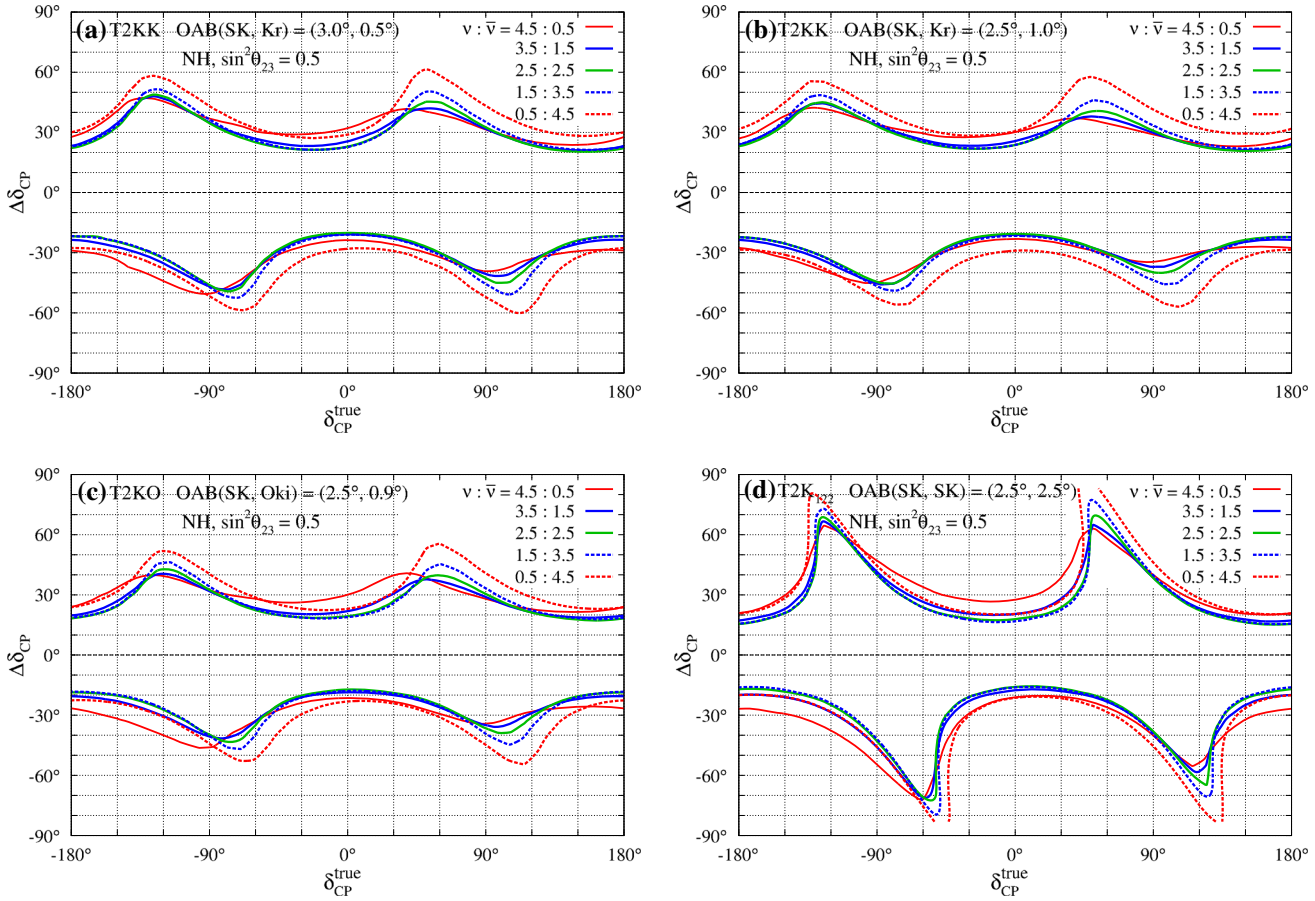

Fig. 11 The uncertainty of CP phase measurements as functions of the CP phase when $\sin^2\theta_{23} = 0.5$, and the mass hierarchy is known to be the normal hierarchy. The *solid-red*, *solid-blue*, *solid-green*, *dashed-blue* and *dashed-red curves* are for the ν_μ–$\bar{\nu}_\mu$ focusing beam ratio of 4.5:0.5, 3.5:1.5, 2.5:2.5, 1.5:3.5, and 0.5:4.5 $\times 10^{21}$ POT with the proton energy of 40 GeV, respectively

ratio, for example, the T2KK and T2KO experiments measure the CP phase with the uncertainty of ∼20°–50° (T2KK with 3.0° OAB at the SK), ∼20°–45° (T2KK with 2.5° OAB at the SK and T2KO) and ∼15°–70° ($\mathrm{T2K}_{122}$), depending on the CP phase.

The effects of including the $\bar{\nu}_\mu$ focusing beam can be understood in terms of correlations of the oscillation parameters between the ν_μ and $\bar{\nu}_\mu$ focusing beams. We illustrate this point taking the $\mathrm{T2K}_{122}$ experiment as an example. In Fig. 12, we show the $\Delta\chi^2$ minimums and pull factors of the oscillation parameters for the different ν_μ–$\bar{\nu}_\mu$ focusing beam ratios as functions of the test δ_{CP}. The pull factor of a fitting parameter X is defined as $(X^{\mathrm{fit}} - X^{\mathrm{input}})/\delta X$, where δX is the uncertainty of the parameter. In the upper-left panel (a), solid-red, dashed-red and dash-dotted blue curves show the $\Delta\chi^2$ minimums for the ν_μ–$\bar{\nu}_\mu$ focusing beam ratios of 5:0, 0:5 and 2.5:2.5 ($\times 10^{21}$ POT with the proton energy of 40 GeV), respectively. Here, the true CP phase is assumed to be 0°, and the mass hierarchy is known to be the normal hierarchy. In the lower plot (c), we show the corresponding pull factors of the oscillation parameters for ν_μ:$\bar{\nu}_\mu$ = 5:0 (upper-half panel) and 0:5 (lower-half panel). We see that each pull factor of $\sin^2 2\theta_{13}$ and $\sin^2\theta_{23}$ shows clear anti-correlation between the ν_μ and $\bar{\nu}_\mu$ focusing beams, i.e., the sign of the each pull factor is opposite between those focusing beams. This is because the sign of those pull factors is mainly related to the sign of the $\sin\delta_{\mathrm{CP}}$ term in the $\nu_\mu \to \nu_e$ oscillation probability (Eq. (2.6b)), which is inverted for the anti-neutrino beam case. Thus, inclusion of the $\bar{\nu}_\mu$ focusing beam would restrict the deviations of $\sin^2 2\theta_{13}$ and $\sin^2\theta_{23}$, resulting in the larger $\Delta\chi^2$ minimum for the 2.5:2.5 beam ratio than 5:0 in the upper panel (a). For the $\delta_{\mathrm{CP}}^{\mathrm{true}} = 60°$ case (right panels in Fig. 12), on the other hand, the anti-correlation of the pull factors is not so evident for $60° \lesssim \delta_{\mathrm{CP}}^{\mathrm{test}} \lesssim 120°$ resulting in the rather reduction of the accuracy of the CP phase measurement when including $\bar{\nu}_\mu$ focusing beams. A similar situation occurs for $\delta_{\mathrm{CP}}^{\mathrm{true}} \sim -60°$ and $\pm 120°$.

In Fig. 13, we show the uncertainties of the CP phase measurements for the inverted hierarchy case. The uncertainties show similar dependences on the ν_μ–$\bar{\nu}_\mu$ focusing

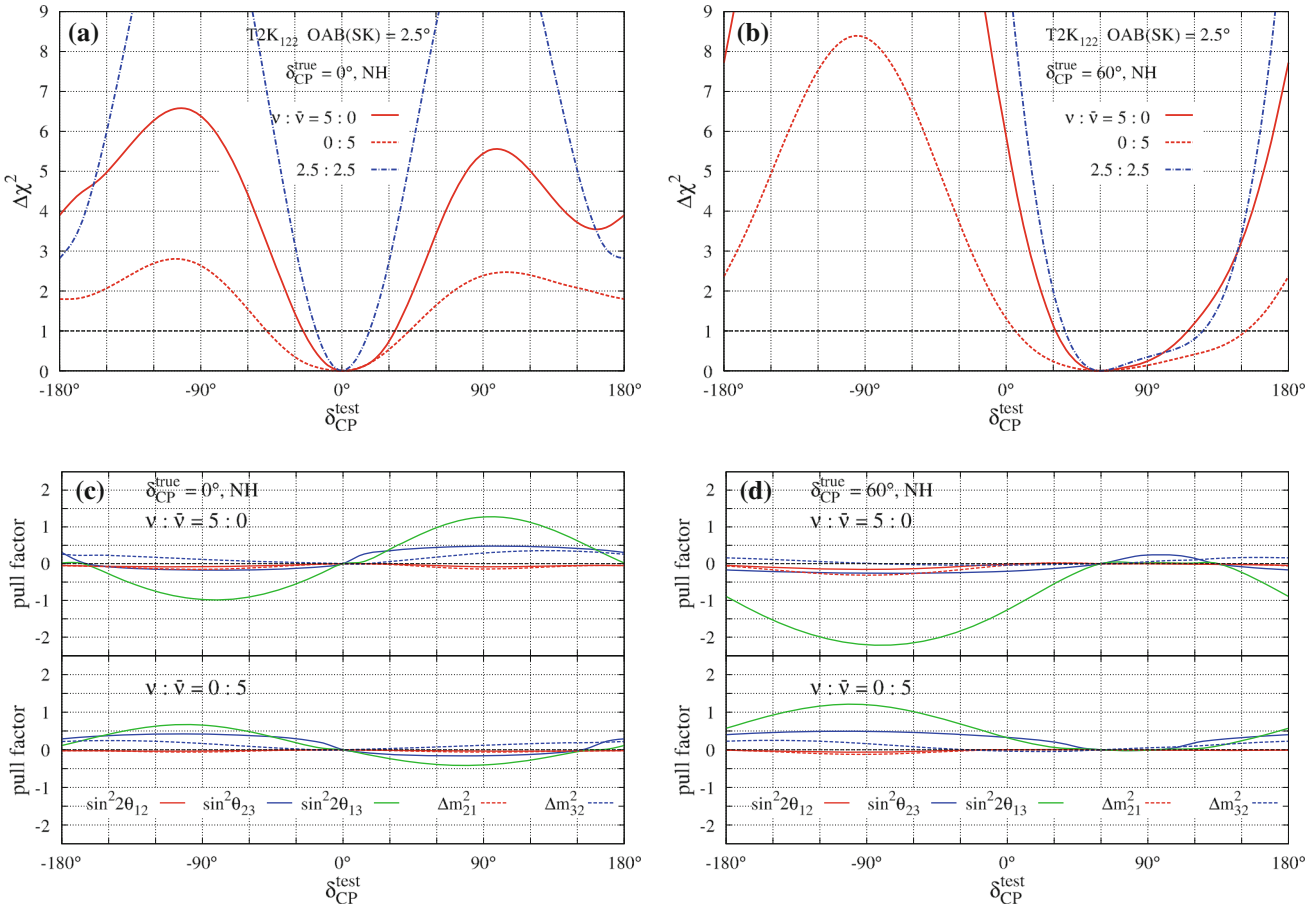

Fig. 12 The $(\Delta\chi^2)_{\rm min}$ (**a**, **b**) and pull factors of the oscillation parameters (**c**, **d**) as functions of the test $\delta_{\rm CP}$ in the T2K$_{122}$ experiment. The *left* (**a**, **c**) and *right* (**b**, **d**) panels are for $\delta_{\rm CP}^{\rm true} = 0°$ and 60°, respectively. *Solid-red*, *dashed-red* and *dash-dotted blue curves* in the panels **a** and **b** show the sensitivity with ν_μ–$\bar{\nu}_\mu$ focusing beam ratio of 5:0, 0:5 and 2.5:2.5 $\times 10^{21}$ POT with the proton energy of 40 GeV, respectively. The *upper-* and *lower-half figures* in the panels **c** and **d** show pull factors with ν_μ:$\bar{\nu}_\mu$ = 5:0 and 0:5, respectively. It is assumed that the mass hierarchy is known to be the normal hierarchy and $\sin^2\theta_{23} = 0.5$

beam ratio as in the normal hierarchy case, showing that the 3.5:1.5–1.5:3.5 beam ratio give the smallest uncertainty except for $\delta_{\rm CP} \sim \pm 60°$ and $\pm 120°$. Using the 2.5:2.5 beam ratio, the T2KK, T2KO, and T2K$_{122}$ experiments measure the CP phase with the uncertainty of ∼20°–50° (T2KK with 3.0° OAB), ∼20°–45° (T2KK with 2.5° OAB), ∼15°–45° (T2KO) and ∼15°–75° (T2K$_{122}$), depending on the CP phase.

We also show the sensitivities to the CP phase measurements in the test-$\delta_{\rm CP}$ vs. true-$\delta_{\rm CP}$ plane in Fig. 14 when $\sin^2\theta_{23} = 0.5$ and the mass hierarchy is known to be the normal hierarchy. The ν_μ–$\bar{\nu}_\mu$ focusing beam ratio is fixed at 2.5:2.5. The solid-red, dashed-blue and dash-dotted-green contours show $(\Delta\chi^2)_{\rm min} = 1, 4, 9$, respectively, for (a) T2KK with 3.0° OAB at the SK and 0.5° OAB at the Kr, (b) T2KK with 2.5° OAB at the SK and 1.0° OAB at the Kr, (c) T2KO and (d) T2K$_{122}$ experiments. We see that both $\delta_{\rm CP}^{\rm test} = 0°$ and 180° are rejected with the significance of $(\Delta\chi^2)_{\rm min} > 9$ for $-100° < \delta_{\rm CP} < -60°$ and $70° < \delta_{\rm CP} < 120°$ by the T2KO experiment and for $-120° < \delta_{\rm CP} < -60°$ and $60° < \delta_{\rm CP} < 120°$ by the T2K$_{122}$ experiment. The T2KK experiment has less sensitivity to the CP violation than the T2KO and T2K$_{122}$ experiments and rejects both $\delta_{\rm CP}^{\rm test} = 0°$ and 180° with the significance of $9 > (\Delta\chi^2)_{\rm min} > 4$ for $-120°(-135°) < \delta_{\rm CP} < -45°$ and $45° < \delta_{\rm CP} < 140°$ for the normal (inverted) hierarchy case. The low sensitivity regions due to the $\delta_{\rm CP}$ and $\pi - \delta_{\rm CP}$ degeneracy of $\sin\delta_{\rm CP}$ can be seen around $\delta_{\rm CP}^{\rm test} = \pi - \delta_{\rm CP}$. We also show the sensitivity plots for the inverted hierarchy case in Fig. 15. The sensitivity is similar to that of the normal hierarchy case with a slight difference due to the relative sign change between the $\sin\delta_{\rm CP}$ and $\cos\delta_{\rm CP}$ terms in the $\nu_\mu \to \nu_e$ and $\bar{\nu}_\mu \to \bar{\nu}_e$ oscillation probability, Eq. (2.6b).

The $\sin^2\theta_{23}$ dependence of the sensitivity to the CP phase measurements is shown in Fig. 16. These are the same sensitivity plots as Fig. 14a but for $\sin^2\theta_{23} = 0.4$ (left plot) and

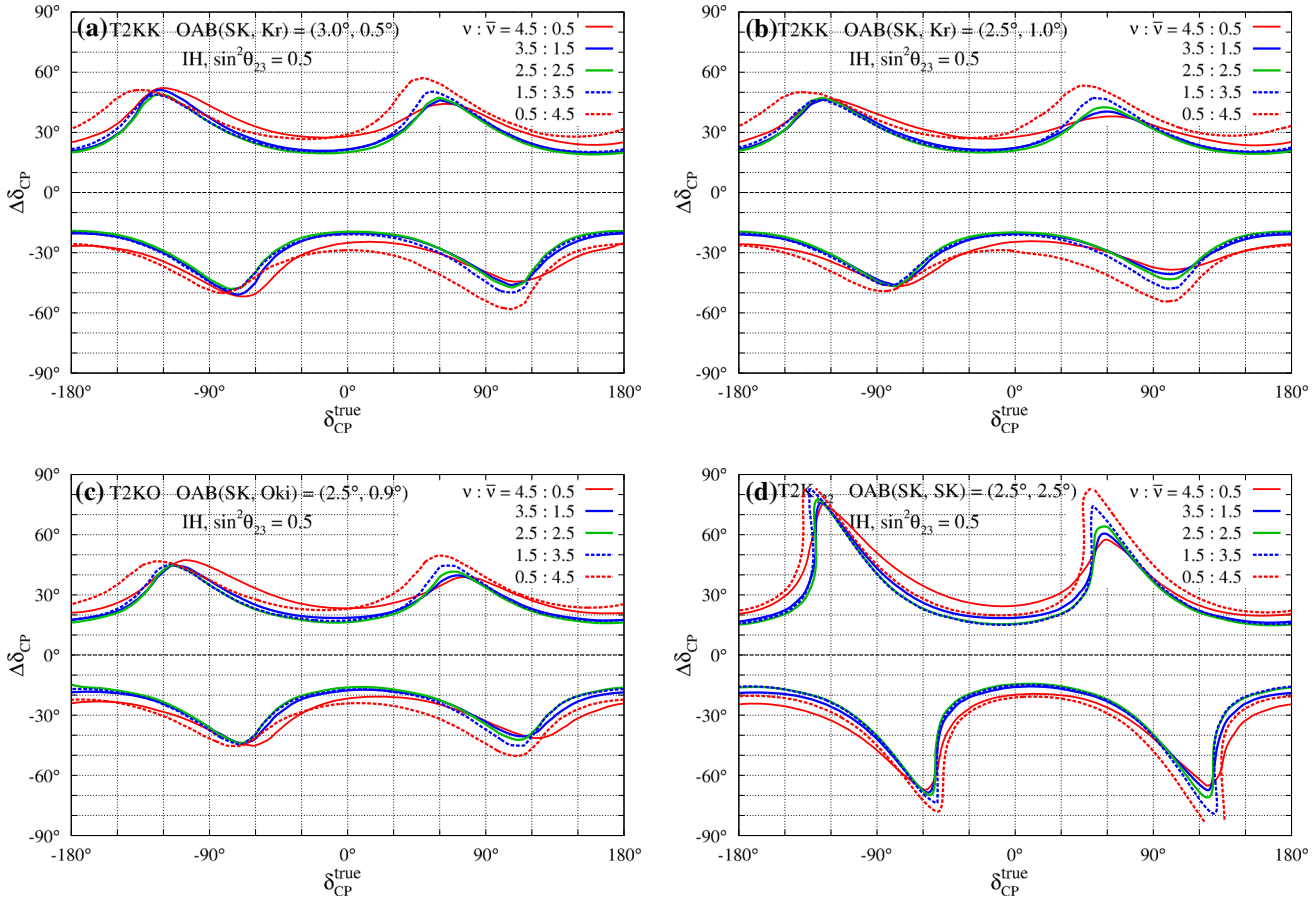

Fig. 13 Same as Fig. 11 but for the inverted hierarchy case

0.6 (right plot) for the T2KK experiment with 3.0° OAB at the SK and 0.5° OAB at the Kr. It is assumed that the mass hierarchy is known to be the normal hierarchy. The sensitivity is better for smaller $\sin^2\theta_{23}$, as shown in the figure. This is because the coefficients of the $\sin\delta_{CP}$ and $\cos\delta_{CP}$ in the $\nu_\mu \to \nu_e$ oscillation probability, Eq. (2.6b), is proportional to $1/\tan\theta_{23}$. The percentages of the regions rejected with $(\Delta\chi^2)_{\min} > 1, 4, 9$ in the test-δ_{CP} vs. true-δ_{CP} plane are 83% (80%), 67% (60%) and 44% (35%), respectively, for $\sin^2\theta_{23} = 0.4\,(0.6)$. Similar dependences are found for the inverted hierarchy case and other experiments.

6 Summary and conclusion

In this paper, we have revisited the previous analysis of Ref. [22,24,25] on the sensitivities to the mass-hierarchy determination and leptonic CP phase measurements of the Tokai-to-Kamioka-and-Korea (T2KK) [15–26] and Tokai-to-Kamioka-and-Oki (T2KO) experiments [25,27], putting emphasis on the ν_μ and $\bar{\nu}_\mu$ focusing beam ratio with dedicated estimation of backgrounds. We place a Super-Kamiokande (SK) type water Čerenkov detector of 100 kton fiducial volume in Korea (T2KK) or Oki island (T2KO) at 1000 km and 653 km away from the J-PARC neutrino facility, respectively. The neutral-current (NC) single-π^0 background and its uncertainty are estimated by using the realistic π^0 rejection probability based on the POLfit algorithm [42], taking into account the coherent π^0 production processes, which is neglected in the previous analysis [22], and including the uncertainty of axial masses in the neutrino–nucleus interaction model [32,33]. The sensitivities are then evaluated using the standard χ^2 analysis.

We found that the wrong mass hierarchy is rejected with $|\overline{\Delta\chi^2_{\rm MH}}| > 10$ in the T2KK and $|\overline{\Delta\chi^2_{\rm MH}}| > 3$ in the T2KO experiment for any CP phases when $\sin^2\theta_{23} = 0.5$, using the ν_μ and $\bar{\nu}_\mu$ focusing beam ratio between 3:2 and 2.5:2.5 (in units of 10^{21}POT with the proton energy of 40 GeV). It should be noted that the $|\overline{\Delta\chi^2_{\rm MH}}|$ quoted in this study is regarded as the average sensitivity expected for an experiment because we neglect the statistical fluctuations in input data set. Although a rigorous interpretation of the $|\overline{\Delta\chi^2_{\rm MH}}|$ needs dedicated statistical consideration, above $|\overline{\Delta\chi^2_{\rm MH}}|$ may be roughly interpreted as the 80% probabilities of determining the mass hierarchy with $>2.6\,\sigma$ for T2KK and $>1.3\,\sigma$ for

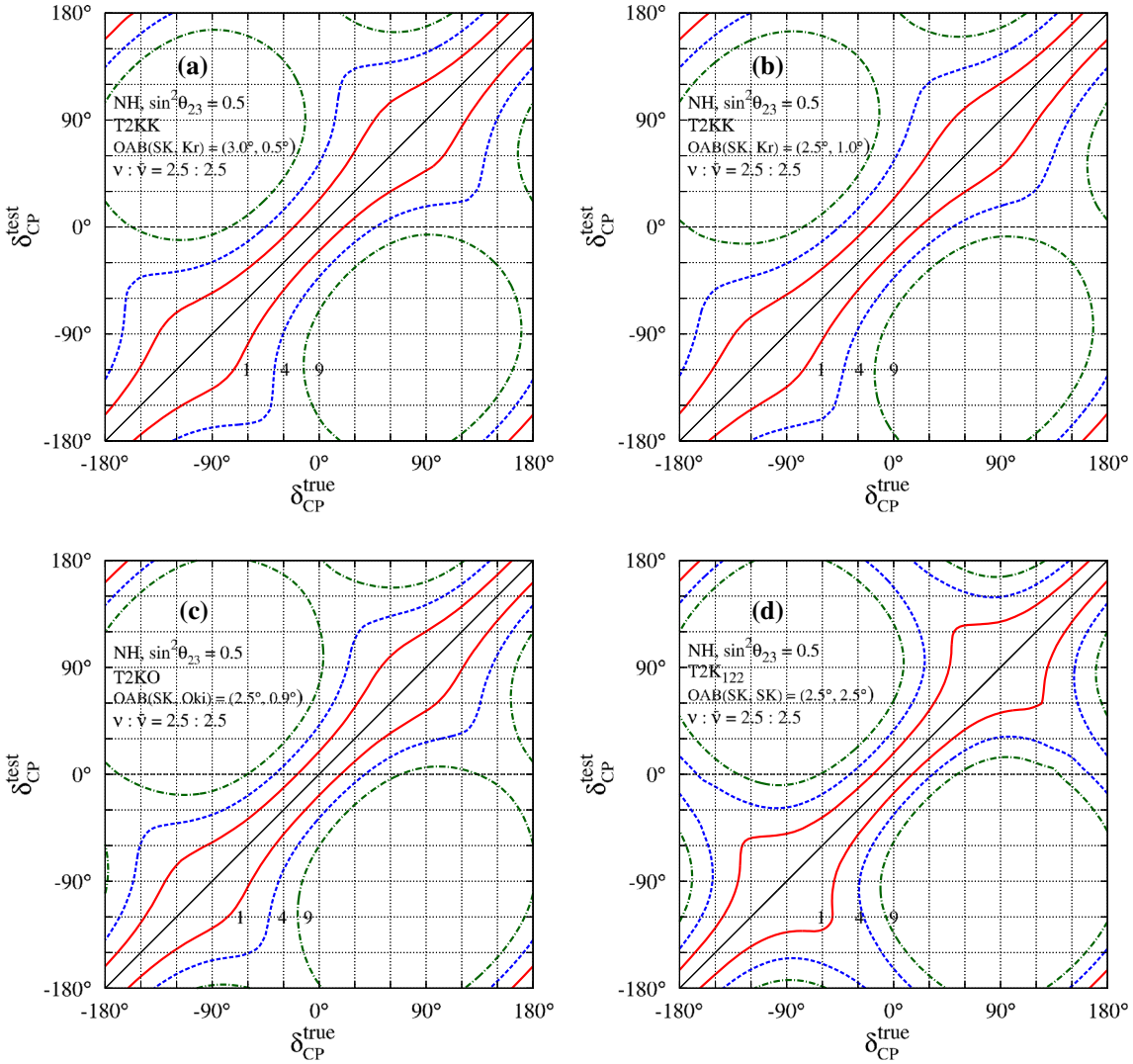

Fig. 14 The sensitivities to the CP phase measurements in the test-δ_{CP} vs. true-δ_{CP} plane when $\sin^2\theta_{23} = 0.5$, and mass hierarchy is known to be the normal hierarchy. **a** T2KK with 3.0° OAB at the SK, **b** T2KK with 2.5° OAB at the SK, **c** T2KO and **d** $T2K_{122}$. The ν_μ–$\bar{\nu}_\mu$ focusing beam ratio is fixed at 2.5:2.5 $\times 10^{21}$POT with the proton energy of 40 GeV. The *solid-red*, *dashed-blue* and *dash-dotted-green contours* show $(\Delta\chi^2)_{\rm min} = 1, 4, 9$, respectively

T2KO, respectively, assuming the Gaussian distribution for the $\Delta\chi^2_{\rm MH}$ in the T2KK and T2KO experiments (see Fig. 2 in Ref. [49] for the interpretation).

In the most sensitive region around $\delta_{CP} \sim -90°$ for the normal hierarchy case, we reject the wrong mass hierarchy with $|\overline{\Delta\chi^2_{\rm MH}}| \sim 32$ in the T2KK experiment (3.0° OAB at the SK) and with $|\overline{\Delta\chi^2_{\rm MH}}| \sim 20$ in the T2KO experiment, using the 3:2–2.5:2.5 beam ratio. These $|\overline{\Delta\chi^2_{\rm MH}}|$ correspond to the 80% probabilities of the mass-hierarchy determination with $>4.9\,\sigma$ for the T2KK experiment and with $>3.8\,\sigma$ for the T2KO experiment. On the other hand, for the inverted hierarchy case, we reject the wrong mass hierarchy with $|\overline{\Delta\chi^2_{\rm MH}}| \sim 30$ in the T2KK experiment (3.0° OAB at the SK) and with $|\overline{\Delta\chi^2_{\rm MH}}| \sim 18$ in the T2KO experiment around $\delta_{CP} \sim 90°$, using the same beam ratio as the normal hierarchy case. These $|\overline{\Delta\chi^2_{\rm MH}}|$ correspond to the 80% probabilities of the mass-hierarchy determination with $>4.7\,\sigma$ for the T2KK experiment and with $>3.6\,\sigma$ for the T2KO experiment. These sensitivities are obtained for $\sin^2\theta_{23} = 0.5$ and enhanced (reduced) by 30–40% in $|\overline{\Delta\chi^2_{\rm MH}}|$ for $\sin^2\theta_{23} = 0.6\,(0.4)$.

We also examined the sensitivity to the CP phase measurements. The ν_μ and $\bar{\nu}_\mu$ focusing beam ratio between 3.5:1.5 and 1.5:3.5 give the smallest uncertainty for most of the CP phases. Employing the 2.5:2.5 beam ratio, the T2KK and T2KO experiments measure the CP phase with the uncertainty of ∼20°–50° (T2KK with 3.0° OAB at the SK), ∼20°–45° (T2KK with 2.5° OAB at the SK and T2KO), depend-

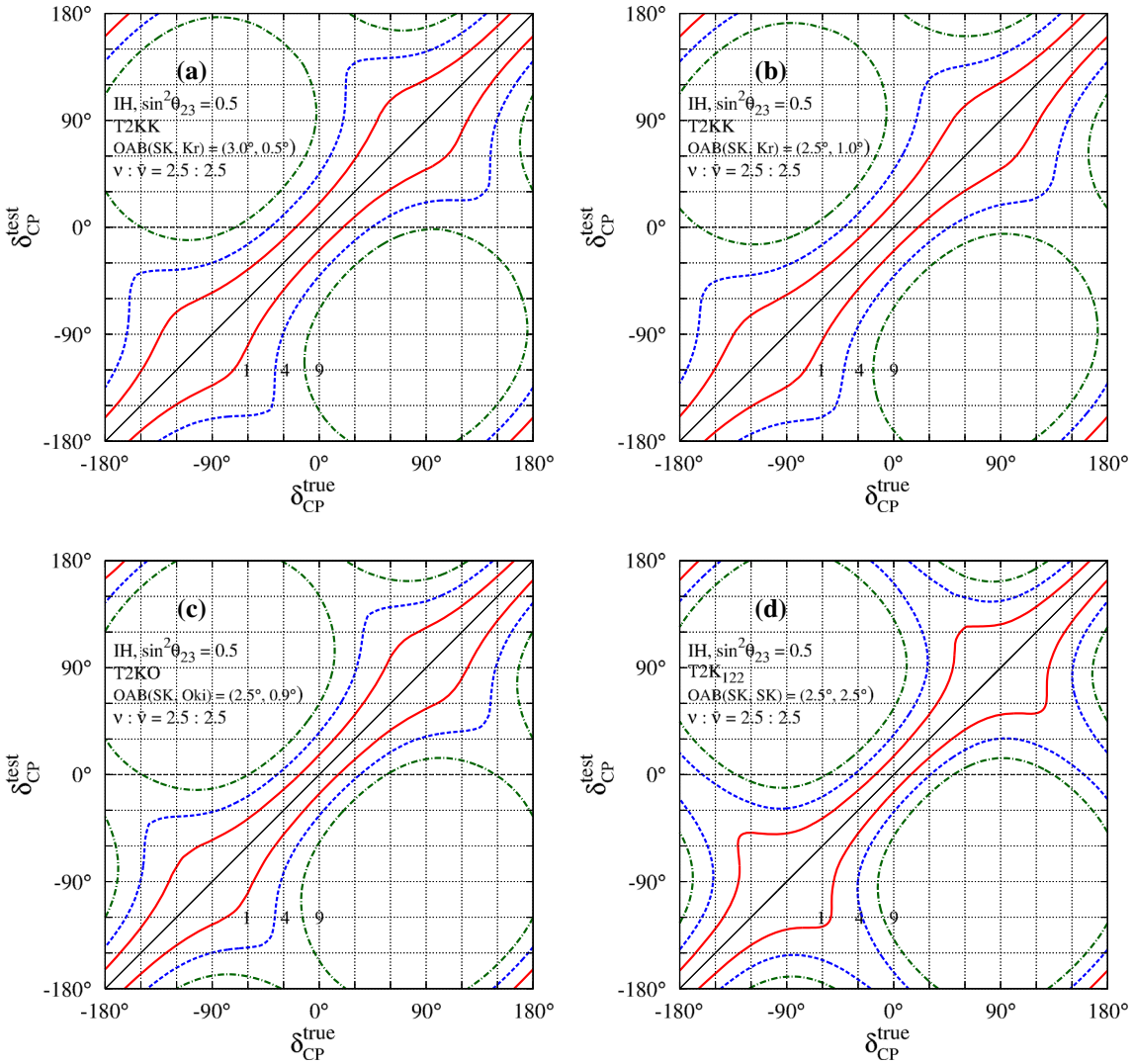

Fig. 15 Same as Fig. 14 but for the inverted hierarchy case

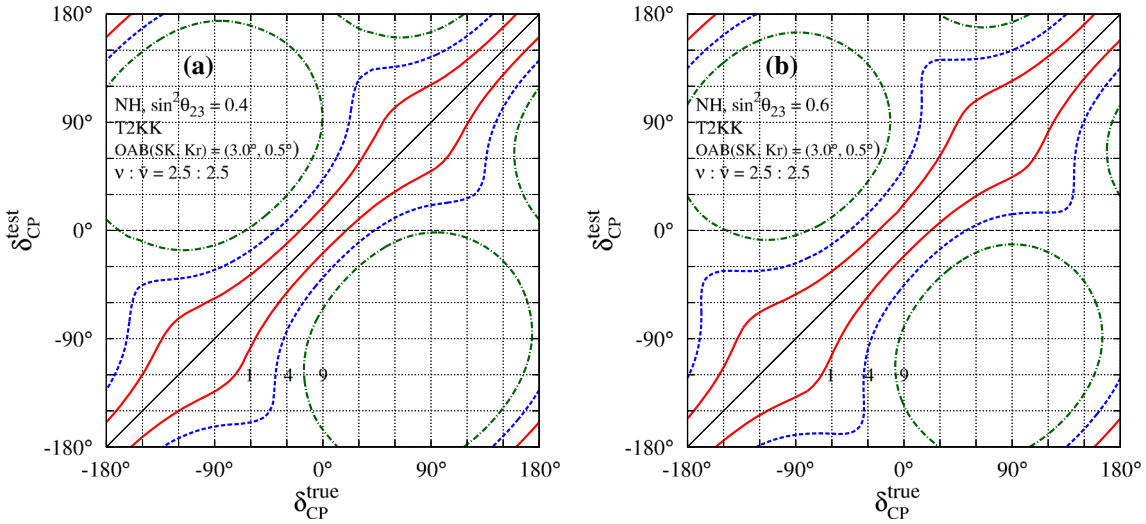

Fig. 16 Same as Fig. 14a but for $\sin^2\theta_{23} = 0.4$ (*left*) and $\sin^2\theta_{23} = 0.6$ (*right*)

ing on the CP phase. We can measure the CP phase most accurately around $\delta_{\rm CP} \sim 0°$ and $\sim 180°$, while the uncertainty is largest around $\delta_{\rm CP} \sim \pm 60°$ and $\sim \pm 120°$. A long baseline is helpful to improve the CP phase measurements around those large uncertainty regions. The mass hierarchy and $\sin^2\theta_{23}$ dependence of the CP phase measurements are not so large. The CP violation in the lepton sector is detected with $(\Delta\chi^2)_{\rm min} > 9$ for $-100° < \delta_{\rm CP} < -60°$ and $70° < \delta_{\rm CP} < 120°$ by the T2KO experiment, while the T2KK experiment detects the CP violation only with $(\Delta\chi^2)_{\rm min} > 4$. In either experiment, we need larger statistics to establish the CP violation in a wide range of the CP phases.

As discussed in this paper, the T2KK and T2KO experiments can improve their sensitivity to both the mass-hierarchy determination and the leptonic CP phase measurement using ν_μ and $\bar{\nu}_\mu$ focusing beams with 3:2–2.5:2.5 beam ratio. This improvement is significant especially for the mass hierarchy determination, lifting the highest sensitivities in the T2KK (both 2.5° and 3.0° OAB at the SK) and T2KO experiments. The lowest sensitivities are improved in the T2KK experiment with 2.5° OAB at the SK, while the improvement is not so evident in the other experiments. The T2KK experiment allows us to determine the mass hierarchy and measure the leptonic CP phase simultaneously. The T2KO experiment also has the sensitivity to the CP phase measurement, while its physics potential for the mass hierarchy determination is not as good as that of the T2KK experiment.

Acknowledgements We would like to thank T. Nakaya and M. Yokoyama for useful discussions and comments on the CP phase sensitivity study of T2K$_{122}$ setup. Y.T. wishes to thank the Korea Neutrino Research Center and KIAS, where part of this work was done. This work is in part supported by the Grant in Aid for Scientific Research No. 25400287 (K.H.) and No. 26400254 (N.O. and Y.T.) from MEXT, Japan, by National Research Foundation of Korea (NRF) Research Grant NRF-2015R1A2A1A05001869 (P.K.), and by the NRF grant funded by the Korea government (MSIP) (No. 2009-0083526) through Korea Neutrino Research Center at Seoul National University (P.K. and Y.T.).

Appendix A: Signal cross sections

We parameterize the CCQE cross sections for oxygen nuclei after imposing the selection criteria (2.10) as follows:

$$\hat{\sigma}^{\rm CCQE}_{\nu O}(E_\nu) = \sigma^{\rm CCQE}_{\nu}(E_\nu) \times \begin{cases} \frac{\alpha^\nu}{1+(\beta^\nu/E_\nu)^8} & (0.2 \le E_\nu < 0.8\,{\rm GeV}), \\ c_0^\nu + c_1^\nu E_\nu + c_2^\nu E_\nu^2 + c_3^\nu E_\nu^3 & (0.8 \le E_\nu \le 5\,{\rm GeV}), \end{cases} \tag{A.1}$$

Table 4 The parameters for the parameterization, Eq. (A.1), of the oxygen CCQE cross sections after imposing the CCQE selection criteria (2.10)

CCQE-O	α	β	c_0	c_1	c_2	c_3
$\nu_\mu = \nu_e$	0.998	0.284	1.02	−0.0323	0.00413	0
$\bar{\nu}_\mu = \bar{\nu}_e$	0.733	0.275	0.718	0.0253	0.00990	0.00107

where ν denotes ν_μ, ν_e, $\bar{\nu}_\mu$ and $\bar{\nu_e}$, and $\sigma_\nu^{\rm CCQE}$ is for the CCQE cross sections for a water target without any cuts [55]; E_ν is in GeV units. The parameters α^ν, β^ν and c^ν's are summarized in Table 4.

The hydrogen CCQE cross sections can be parameterized as

$$\hat{\sigma}^{\rm CCQE}_{\bar{\nu}_{\mu/e}H}(E_\nu) = \sigma^{\rm CCQE}_{\bar{\nu}_{\mu/e}}(E_\nu) \times \begin{cases} 0.324 - 0.116E_\nu & (0.2 \le E_\nu < 0.8\,{\rm GeV}), \\ 0.271 - 0.0580E_\nu & \\ \quad +0.0172E_\nu^2 - 0.00169E_\nu^3 & (0.8 \le E_\nu \le 5\,{\rm GeV}). \end{cases} \tag{A.2}$$

Note that only anti-neutrinos interact with hydrogens via the CCQE interactions.

The non-CCQE signal cross sections, $\hat{\sigma}^{\rm nonCCQE}_{\nu Z}(E_\nu)$, are the total cross sections of all the non-CCQE events that satisfy the CCQE selection criteria (2.10) and can be parameterized for the ν–O and $\bar{\nu}$–O interactions as

$$\hat{\sigma}^{\rm nonCCQE}_{\nu O}(E_\nu) = \sigma^{\rm CCQE}_{\nu}(E_\nu) \times \begin{cases} \frac{\alpha^\nu}{1+(\beta^\nu/E_\nu)^5} & (0.2 \le E_\nu < 1.1\,{\rm GeV}), \\ c_0^\nu + c_1^\nu E_\nu + c_2^\nu E_\nu^2 + c_3^\nu E_\nu^3 & (1.1 \le E_\nu \le 5\,{\rm GeV}), \end{cases} \tag{A.3}$$

and for the ν–H and $\bar{\nu}$–H interactions as

$$\hat{\sigma}^{\rm nonCCQE}_{\nu_{\mu/e}H}(E_\nu) = \sigma^{\rm CCQE}_{\nu}(E_\nu) \times \begin{cases} \frac{\alpha^\nu}{1+(\beta^\nu/E_\nu)^5} & (0.2 \le E_\nu < 1.1\,{\rm GeV}), \\ c_0^\nu + c_1^\nu E_\nu + c_2^\nu E_\nu^2 + c_3^\nu E_\nu^3 & (1.1 \le E_\nu \le 5\,{\rm GeV}), \end{cases} \tag{A.4a}$$

$$\hat{\sigma}^{\rm nonCCQE}_{\bar{\nu}_{\mu/e}H}(E_\nu) = \sigma^{\rm CCQE}_{\bar{\nu}}(E_\nu) \times \begin{cases} \frac{\alpha^{\bar{\nu}}}{1+(\beta^{\bar{\nu}}/E_\nu)^{10}} & (0.2 \le E_\nu < 0.6\,{\rm GeV}), \\ c_0^{\bar{\nu}} + c_1^{\bar{\nu}} E_\nu + c_2^{\bar{\nu}} E_\nu^2 + c_3^{\bar{\nu}} E_\nu^3 & (0.6 \le E_\nu \le 5\,{\rm GeV}). \end{cases} \tag{A.4b}$$

The parameters α^ν, β^ν and c^ν are summarized in Table 5.

We find that those parameterizations reproduce well the results of `Nuance` for $E_\nu \le 5$ GeV.

Table 5 Same as Table 4 but for the non-CCQE neutrino–nucleus interactions, Eqs. (A.3) and (A.4)

	α	β	c_0	c_1	c_2	c_3
nonCCQE-O						
ν_μ	0.418	0.820	0.0429	0.355	−0.0767	0.00608
ν_e	0.434	0.764	0.0318	−0.403	−0.0921	0.00753
$\bar{\nu}_\mu$	0.232	0.747	−0.0433	0.291	−0.0648	0.00524
$\bar{\nu}_e$	0.242	0.688	−0.0289	0.301	−0.0691	0.00571
nonCCQE-H						
ν_μ	0.0396	0.676	0.0184	0.0230	−0.00669	0.000674
ν_e	0.0422	0.637	0.0286	0.0127	−0.00262	0.000183
$\bar{\nu}_\mu$	0.0213	0.484	0.0259	−0.00877	0.00274	−0.000271
$\bar{\nu}_e$	0.0238	0.463	0.0244	−0.00538	0.00152	−0.000142

Appendix B: Smearing functions $S^X_{\bar{\nu}_\alpha Z}(E_\nu, E_{\rm rec})$

In this appendix, we show our parameterizations of the smearing functions, $S^X_{\bar{\nu}_\alpha Z}(E_\nu, E_{\rm rec})$, which map the incoming anti-neutrino energy, E_ν, onto the reconstructed energy, $E_{\rm rec}$, for the charged-current (CC) events. Smearing functions for neutrinos was already constructed in Ref. [22]. The superscript X denotes the event type, X = CCQE for the charged-current quasi-elastic (CCQE) events or X = non-CCQE for the other CC events that pass the CCQE selection criteria of Eq. (2.10). The subscript $\bar{\nu}_\alpha$ and Z denote an incoming anti-neutrino ($\bar{\nu}_\mu$ and $\bar{\nu}_e$) and a target nucleus, respectively. These functions take account of the Fermi motion of target nucleons inside an oxygen nucleus and the finite detector resolutions for muons and electrons in a water Čerenkov detector and valid in the region of 0.3 GeV $\leq E_\nu \leq$ 5.0 GeV for 0.4 GeV $\leq E_{\rm rec} \leq$ 6.0 GeV.

B.1 CCQE events

B.1.1 ^{16}O interaction

The $E_{\rm rec}$ distributions of the anti-neutrino induced CCQE events via interactions with oxygen nuclei, which are generated by `Nuance` v.3.504 package [40], can be parameterized by three Gaussians,

$$S^{\rm CCQE}_{\bar{\nu}_\alpha O}(E_\nu, E_{\rm rec}) = \frac{1}{A^\alpha(E_\nu)} \sum_{n=1}^{3} r_n^\alpha(E_\nu) \times \exp\left\{ -\frac{(E_{\rm rec} - E_\nu + \delta E_n^\alpha(E_\nu))^2}{2(\sigma_n^\alpha(E_\nu))^2} \right\}. \quad \text{(B.1)}$$

Here the incoming anti-neutrino energy, E_ν, and $E_{\rm rec}$ are in MeV units. Each function is normalized by

$$A^\alpha(E_\nu) = \sqrt{2\pi} \sum_{n=1}^{3} r_n^\alpha(E_\nu)\sigma_n^\alpha(E_\nu). \quad \text{(B.2)}$$

For the $\bar{\nu}_\mu$ case, the weight factors r_n^α, variances σ_n^α, and the energy shifts δE_n^α, are functions of the dimensionless parameter, $z \equiv E_\nu/(1000\,{\rm MeV})$, and expressed as

$$\begin{aligned} r_1^\mu &= 3.20 - 2.16\, z + 0.562\, z^2 - 0.0504\, z^3, \\ r_2^\mu &= 2.05 - 1.52\, z + 0.406\, z^2 - 0.0360\, z^3, \\ r_3^\mu &= 0.110 - 0.0828\, z + 0.0224\, z^2 - 0.00198\, z^3, \quad \text{(B.3)} \\ \sigma_1^\mu &= 11.3 + 27.4\, z - 1.01\, z^2, \\ \sigma_2^\mu &= 36.0 + 49.0\, z - 3.31\, z^2, \\ \sigma_3^\mu &= -18.0 + 241\, z - 56.8\, z^2 + 4.85\, z^3, \quad \text{(B.4)} \\ \delta E_1^\mu &= 43.5 - 9.64\, z + 2.86\, z^2 - 0.229\, z^3, \\ \delta E_2^\mu &= 28.1 - 2.89\, z - 0.482\, z^2, \\ \delta E_3^\mu &= -4.84 - 5.34\, z - 1.59\, z^2. \quad \text{(B.5)} \end{aligned}$$

The variances and the energy-shift terms δE_n^μ are given in units of MeV.

For the $\bar{\nu}_e$ case, we find

$$\begin{aligned} r_1^e &= 1, \\ r_2^e &= 0.586 - 0.258\, z + 0.122\, z^2 - 0.0137\, z^3, \\ r_3^e &= 0.0140 - 0.00131\, z + 0.00502\, z^2, \quad \text{(B.6)} \\ \sigma_1^e &= 23.3 + 25.8\, z - 1.54\, z^2, \\ \sigma_2^e &= 53.8 + 46.5\, z - 2.79\, z^2, \\ \sigma_3^e &= 12.5 + 250\, z - 66.1\, z^2 + 6.43\, z^3, \quad \text{(B.7)} \\ \delta E_1^e &= 42.9 - 11.0\, z + 4.42\, z^2 - 0.382\, z^3, \\ \delta E_2^e &= 27.3 - 6.43\, z, \\ \delta E_3^e &= -176 + 178\, z - 86.5\, z^2 + 15.5\, z^3 - 1.04\, z^4. \quad \text{(B.8)} \end{aligned}$$

B.1.2 Proton interaction

The $E_{\rm rec}$ distributions of the $\bar{\nu}_\mu$ induced CCQE events via interactions with protons can be parameterized by up to two Gaussians,

$$S^{\mathrm{CCQE}}_{\bar{\nu}_\mu H}(E_\nu, E_{\mathrm{rec}}) = \frac{1}{A^\alpha(E_\nu)}\Big[r_1^\alpha(E_\nu) \times \exp\left\{-\frac{(E_{\mathrm{rec}} - E_\nu + \delta E_1^\alpha(E_\nu))^2}{2(\sigma_1^\alpha(E_\nu))^2}\right\} + r_2^\alpha(E_\nu)\exp\left\{-\frac{(E_{\mathrm{rec}} - E_\nu + \delta E_2^\alpha(E_\nu))^2}{2(\sigma_2^\alpha(E_\nu))^2}\right\} \times \Theta(z - 0.7)\Big], \tag{B.9}$$

where Θ is a step function. The weight factors r_n^α, variances σ_n^α (MeV) and energy shifts δE_n^α (MeV) are expressed as

$$\begin{aligned} r_1^\mu &= 1, \\ r_2^\mu &= 0.106, \end{aligned} \tag{B.10}$$

$$\begin{aligned} \sigma_1^\mu &= 3.20 + 25.5\,z, \\ \sigma_2^\mu &= -3.73 + 52.7\,z, \end{aligned} \tag{B.11}$$

$$\begin{aligned} \delta E_1^\mu &= 0.00, \\ \delta E_2^\mu &= 11.6 - 17.0\,z. \end{aligned} \tag{B.12}$$

For the $\bar{\nu}_e$ case, the E_{rec} distributions are parameterized by up to three Gaussians,

$$S^{\mathrm{CCQE}}_{\bar{\nu}_e H}(E_\nu, E_{\mathrm{rec}}) = \frac{1}{A^\alpha(E_\nu)}\left[r_1^\alpha(E_\nu)\exp\left\{-\frac{(E_{\mathrm{rec}} - E_\nu + \delta E_1^\alpha(E_\nu))^2}{2(\sigma_1^\alpha(E_\nu))^2}\right\}\right. \tag{B.13}$$

$$+ r_2^\alpha(E_\nu)\exp\left\{-\frac{(E_{\mathrm{rec}} - E_\nu + \delta E_2^\alpha(E_\nu))^2}{2(\sigma_2^\alpha(E_\nu))^2}\right\} \tag{B.14}$$

$$\left. + r_3^\alpha(E_\nu)\exp\left\{-\frac{(E_{\mathrm{rec}} - E_\nu + \delta E_3^\alpha(E_\nu))^2}{2(\sigma_3^\alpha(E_\nu))^2}\right\}\Theta(z - 1.0)\right]. \tag{B.15}$$

The weight factors, variances σ_n^α (MeV), and energy shifts δE_n^α (MeV) are

$$\begin{aligned} r_1^e &= 1, \\ r_2^e &= 4.47(e^{0.114\,z-2.59} - e^{-0.698\,z-2.36}), \\ r_3^e &= 0.00532\,e^{0.620\,z}, \end{aligned} \tag{B.16}$$

$$\begin{aligned} \sigma_1^e &= 268(e^{-0.0225\,z} - e^{-0.135\,z-0.0470}), \\ \sigma_2^e &= 297(1 - e^{-0.235\,z}), \\ \sigma_3^e &= 4.41(e^{0.0584\,z+4.27} - e^{-0.489\,z+4.47}), \end{aligned} \tag{B.17}$$

$$\begin{aligned} \delta E_1^e &= \frac{18.3}{1 + 34.0\,e^{-1.02\,z}}, \\ \delta E_2^e &= -7.26 - 5.66\,z, \\ \delta E_3^e &= 665(e^{-0.261\,z+0.0811} - e^{-0.107\,z}). \end{aligned} \tag{B.18}$$

B.2 Non-CCQE events

B.2.1 ^{16}O interaction

The E_{rec} distributions of the anti-neutrino induced non-CCQE events via interactions with oxygen nuclei can be parameterized by up to four Gaussians,

$$S^{\mathrm{nonCCQE}}_{\bar{\nu}_\alpha O}(E_\nu, E_{\mathrm{rec}}) = \frac{1}{A^\alpha(E_\nu)} \times \left[r_1^\alpha(E_\nu)\exp\left\{-\frac{(E_{\mathrm{rec}} - E_\nu + \delta E_1^\alpha(E_\nu))^2}{2(\sigma_1^\alpha(E_\nu))^2}\right\}\right. + r_2^\alpha(E_\nu)\exp\left\{-\frac{(E_{\mathrm{rec}} - E_\nu + \delta E_2^\alpha(E_\nu))^2}{2(\sigma_2^\alpha(E_\nu))^2}\right\}\Theta(z - 0.7) + r_3^\alpha(E_\nu)\exp\left\{-\frac{(E_{\mathrm{rec}} - E_\nu + \delta E_3^\alpha(E_\nu))^2}{2(\sigma_3^\alpha(E_\nu))^2}\right\}\Theta(z - 1.0) + r_4^\alpha(E_\nu)\exp\left\{-\frac{(E_{\mathrm{rec}} - E_\nu + \delta E_4^\alpha(E_\nu))^2}{2(\sigma_4^\alpha(E_\nu))^2}\right\}\left.\Theta(1.5 - z)\right]. \tag{B.19}$$

Each function is normalized as in Eq. (B.2). The fourth Gaussian takes into account the effects of the event selection cut.

For the $\bar{\nu}_\mu$ case, the weight factors r_n^α, variances σ_n^α (MeV) and energy shifts δE_n^α (MeV) are

$$\begin{aligned} r_1^\mu &= 1, \\ r_2^\mu &= 0.325 - 0.0652\,z + 0.0142\,z^2, \\ r_3^\mu &= 0.0804 - 0.00176\,z + 0.00194\,z^2, \\ r_4^\mu &= -0.326 + 0.229\,z, \end{aligned} \tag{B.20}$$

$$\begin{aligned} \sigma_1^\mu &= 70.3 + 13.9\,z, \\ \sigma_2^\mu &= 114 + 40.1\,z, \\ \sigma_3^\mu &= 452(e^{0.0105\,z} - e^{-1.67\,z+1.98}), \\ \sigma_4^\mu &= 111(e^{-1.67\,z} - e^{-323\,z}), \end{aligned} \tag{B.21}$$

$$\begin{aligned} \delta E_1^\mu &= 355, \\ \delta E_2^\mu &= \frac{539}{1 + 1.53\,e^{-2.76\,z}}, \\ \delta E_3^\mu &= 850 + 32\,z, \\ \delta E_4^\mu &= -214 + 998\,z. \end{aligned} \tag{B.22}$$

For the $\bar{\nu}_e$ case, we find

$$\begin{aligned} r_1^e &= 1, \\ r_2^e &= 0.143 + 0.0605\,z, \\ r_3^e &= -0.0459 + 0.105\,z - 0.0134\,z^2, \\ r_4^e &= 0, \end{aligned} \tag{B.23}$$

$$\begin{aligned} \sigma_1^e &= 72.9 + 12.8\,z, \\ \sigma_2^e &= 105 + 40.2\,z, \\ \sigma_3^e &= 147 + 92.7\,z, \end{aligned} \tag{B.24}$$

$$\delta E_1^e = 348 + 0.352\,z,$$

$$\delta E_2^e = \frac{443}{1 - 0.434\, e^{-0.902\, z}},$$
$$\delta E_3^e = 753 + 17.6\, z. \tag{B.25}$$

B.2.2 Proton interaction

The $E_{\rm rec}$ distributions of the $\bar{\nu}_\mu$ induced non-CCQE events via interactions with protons can be parameterized by up to four Gaussians,

$$S^{\rm nonCCQE}_{\bar{\nu}_\mu H}(E_\nu, E_{\rm rec}) = \frac{1}{A^\alpha(E_\nu)} \times \left[r_1^\alpha(E_\nu) \exp\left\{ -\frac{(E_{\rm rec} - E_\nu + \delta E_1^\alpha(E_\nu))^2}{2(\sigma_1^\alpha(E_\nu))^2} \right\} + r_2^\alpha(E_\nu) \exp\left\{ -\frac{(E_{\rm rec} - E_\nu + \delta E_2^\alpha(E_\nu))^2}{2(\sigma_2^\alpha(E_\nu))^2} \right\} + r_3^\alpha(E_\nu) \exp\left\{ -\frac{(E_{\rm rec} - E_\nu + \delta E_3^\alpha(E_\nu))^2}{2(\sigma_3^\alpha(E_\nu))^2} \right\} + r_4^\alpha(E_\nu) \exp\left\{ -\frac{(E_{\rm rec} - E_\nu + \delta E_4^\alpha(E_\nu))^2}{2(\sigma_4^\alpha(E_\nu))^2} \right\} \Theta(z - 1.0) \right]. \tag{B.26}$$

The function is normalized as in Eq. (B.2). The fourth Gaussian parameterizes the long low-energy tail of the distribution. The weight factors r_n^α, variances σ_n^α (MeV) and energy shifts δE_n^α (MeV) are

$$\begin{aligned} r_1^\mu &= e^{-0.442\, z} + 7.84 e^{-2.90\, z}, \\ r_2^\mu &= 1.7 e^{-0.912\, z}, \\ r_3^\mu &= 0.893 e^{-1.53\, z}, \\ r_4^\mu &= 0.0624(e^{-0.352\, z} - e^{-0.434\, z + 0.0365}), \end{aligned} \tag{B.27}$$

$$\begin{aligned} \sigma_1^\mu &= 18.0 + 22.8\, z, \\ \sigma_2^\mu &= 8.61 + 13.5\, z, \\ \sigma_3^\mu &= 31.5 + 46.6\, z - 6.27\, z^2, \\ \sigma_4^\mu &= -498 + 763\, z - 203\, z^2 + 18.7\, z^3, \end{aligned} \tag{B.28}$$

$$\begin{aligned} \delta E_1^\mu &= 212 + 3.81\, z - 0.536\, z^2, \\ \delta E_2^\mu &= 202 - 1.63\, z, \\ \delta E_3^\mu &= 284 - 6.23\, z + 16.1\, z^2, \\ \delta E_4^\mu &= 655 + 35\, z. \end{aligned} \tag{B.29}$$

For the $\bar{\nu}_e$ case, $E_{\rm rec}$ distributions are also parameterized by up to four Gaussians,

$$S^{\rm nonCCQE}_{\bar{\nu}_e H}(E_\nu, E_{\rm rec}) = \frac{1}{A^\alpha(E_\nu)} \times \left[r_1^\alpha(E_\nu) \exp\left\{ -\frac{(E_{\rm rec} - E_\nu + \delta E_1^\alpha(E_\nu))^2}{2(\sigma_1^\alpha(E_\nu))^2} \right\} + r_2^\alpha(E_\nu) \exp\left\{ -\frac{(E_{\rm rec} - E_\nu + \delta E_2^\alpha(E_\nu))^2}{2(\sigma_2^\alpha(E_\nu))^2} \right\} + r_3^\alpha(E_\nu) \exp\left\{ -\frac{(E_{\rm rec} - E_\nu + \delta E_3^\alpha(E_\nu))^2}{2(\sigma_3^\alpha(E_\nu))^2} \right\} + r_4^\alpha(E_\nu) \exp\left\{ -\frac{(E_{\rm rec} - E_\nu + \delta E_4^\alpha(E_\nu))^2}{2(\sigma_4^\alpha(E_\nu))^2} \right\} \Theta(z - 1.5) \right]. \tag{B.30}$$

The weight factors, variances σ_n^α (MeV), and energy shifts δE_n^α (MeV) are

$$\begin{aligned} r_1^e &= 1 + 6.60\, e^{-1.51\, z}, \\ r_2^e &= 2.27\, e^{-2.76\, z} + 0.507\, e^{-0.247\, z}, \\ r_3^e &= 0.0117\, e^{0.196\, z} + 0.375\, e^{-3.88\, z}, \\ r_4^e &= 0.0122\, e^{0.003\, z}, \end{aligned} \tag{B.31}$$

$$\begin{aligned} \sigma_1^e &= 17.0 + 23.9\, z - 1.16\, z^2, \\ \sigma_2^e &= 29.5 + 46.2\, z - 1.70\, z^2, \\ \sigma_3^e &= -162 + 345\, z - 42.6\, z^2, \\ \sigma_4^e &= 62.6\, e^{0.651\, z}, \end{aligned} \tag{B.32}$$

$$\begin{aligned} \delta E_1^e &= 206, \\ \delta E_2^e &= 272 - 3.13\, e^{0.682\, z}, \\ \delta E_3^e &= 210 + 387\, z - 60\, z^2, \\ \delta E_4^e &= -1.43 \times 10^3 + 1.66 \times 10^3\, z - 118\, z^2. \end{aligned} \tag{B.33}$$

References

1. F.P. An et al. (Daya Bay Collaboration), Phys. Rev. Lett. **108**, 171803 (2012). arXiv:1203.1669
2. F. An et al. (Daya Bay Collaboration), Chin. Phys. C **37**, 011001 (2013). arXiv:1210.6327
3. F. An et al. (Daya Bay Collaboration), Phys. Rev. Lett. **112**, 061801 (2014). arXiv:1310.6732
4. F.P. An et al. (Daya Bay Collaboration), Phys. Rev. D **90**, 071101 (2014). arXiv:1406.6468
5. F.P. An et al. (Daya Bay Collaboration), Phys. Rev. Lett.**115**, 111802 (2015). arXiv:1505.03456
6. F.P. An et al. (Daya Bay Collaboration), Phys. Rev. D **93**, 072011 (2016). arXiv:1603.03549
7. J.K. Ahn et al. (RENO Collaboration), Phys. Rev. Lett. **108**, 191802 (2012). arXiv:1204.0626
8. J.H. Choi et al. (RENO Collaboration), Phys. Rev. Lett. **116**, 211801 (2016). arXiv:1511.05849
9. Y. Abe et al. (Double Chooz Collaboration), Phys. Rev. D **86**, 052008 (2012). arXiv:1207.6632
10. Y. Abe et al. (Double Chooz Collaboration), Phys. Lett. B **723**, 66 (2013). arXiv:1301.2948
11. Y. Abe et al. (Double Chooz Collaboration), Phys. Lett. B **735**, 51 (2014). arXiv:1401.5981
12. Y. Abe et al. (Double Chooz Collaboration), JHEP **1410**, 086 (2014). arXiv:1406.7763
13. Y. Abe et al. (Double Chooz Collaboration), JHEP **01**, 163 (2016). arXiv:1510.08937
14. Z. Maki, M. Nakagawa, S. Sakata, Prog. Theor. Phys. **28**, 870 (1962)
15. K. Hagiwara, Nucl. Phys. Proc. Suppl. **137**, 84 (2004). arXiv:hep-ph/0410229

16. M. Ishitsuka, T. Kajita, H. Minakata, H. Nunokawa, Phys. Rev. D **72**, 033003 (2005). arXiv:hep-ph/0504026
17. K. Hagiwara, N. Okamura, K.-I. Senda, Phys. Lett. B **637**, 266 (2006). arXiv:hep-ph/0504061
18. K. Hagiwara, N. Okamura, K.-I. Senda, Phys. Rev. D **76**, 093002 (2007). arXiv:hep-ph/0607255
19. T. Kajita, H. Minakata, S. Nakayama, H. Nunokawa, Phys. Rev. D **75**, 013006 (2007). arXiv:hep-ph/0609286
20. K. Hagiwara, N. Okamura, JHEP **0801**, 022 (2008). arXiv:hep-ph/0611058
21. P. Huber, M. Mezzetto, T. Schwetz, JHEP **0803**, 021 (2008). arXiv:0711.2950
22. K. Hagiwara, N. Okamura, JHEP **0907**, 031 (2009). arXiv:0901.1517
23. F. Dufour, T. Kajita, E. Kearns, K. Okumura, Phys. Rev. D **81**, 093001 (2010). arXiv:1001.5165
24. K. Hagiwara, N. Okamura, K. Senda, JHEP **1109**, 082 (2011). arXiv:1107.5857
25. K. Hagiwara, T. Kiwanami, N. Okamura, K.-I. Senda, JHEP **06**, 036 (2013). arXiv:1209.2763
26. F. Dufour (2012). arXiv:1211.3884
27. A. Badertscher, T. Hasegawa, T. Kobayashi, A. Marchionni, A. Meregaglia et al. (2008). arXiv:0804.2111
28. E. Ciuffoli, J. Evslin, X. Zhang, JHEP **12**, 051 (2014). arXiv:1401.3977
29. J. Evslin, S.-F. Ge, K. Hagiwara, JHEP **02**, 137 (2016). arXiv:1506.05023
30. S.-F. Ge, P. Pasquini, M. Tortola, J.W.F. Valle (2016). arXiv:1605.01670
31. T. Barszczak, Ph.D. thesis, University of California, Irvine (2005)
32. D. Rein, L.M. Sehgal, Ann. Phys. **133**, 79 (1981)
33. D. Rein, L.M. Sehgal, Nucl. Phys. B **223**, 29 (1983)
34. J. Beringer et al. (Particle Data Group), Phys. Rev. D **86**, 010001 (2012)
35. Y. Itow et al. (T2K Collaboration), 239 (2001). arXiv:hep-ex/0106019
36. J. Arafune, M. Koike, J. Sato, Phys. Rev. D **56**, 3093 (1997). arXiv:hep-ph/9703351
37. A.K. Ichikawa, Private communication; the flux data for various off-axis angles are available from the web page: http://www2.yukawa.kyoto-u.ac.jp/~okamura/T2KK/. Some beam profiles are obtained with interpolations by ourselves
38. K. Abe et al. (T2K Collaboration), Nucl. Instrum. Methods A **659**, 106 (2011). arXiv:1106.1238
39. K. Abe et al. (T2K Collaboration), Phys. Rev. Lett. **112**, 061802 (2014). arXiv:1311.4750
40. D. Casper, Nucl. Phys. Proc. Suppl. **112**, 161 (2002). arXiv:hep-ph/0208030
41. Y. Ashie et al. (Super-Kamiokande Collaboration), Phys. Rev. D **71**, 112005 (2005). arXiv:hep-ex/0501064
42. K. Okumura, π^0 rejection with POLfit in SK. Talk at ANT11 in Philadelphia, USA (2011)
43. K. Abe et al. (T2K Collaboration), Phys. Rev. D **91**, 072010 (2015). arXiv:1502.01550
44. A. Kaboth (Collaboration A. Kaboth for the T2K) (2013). arXiv:1310.6544
45. A. Aguilar-Arevalo et al. (MiniBooNE Collaboration), Phys. Rev. D **81**, 092005 (2010). arXiv:1002.2680
46. C. Zhang (Daya Bay Collaboration) (2015). arXiv:1501.04991
47. S.-F. Ge, K. Hagiwara, N. Okamura, Y. Takaesu, JHEP **1305**, 131 (2013). arXiv:1210.8141
48. X. Qian, A. Tan, W. Wang, J. J. Ling, R. D. McKeown, C. Zhang, Phys. Rev. D **86**, 113011 (2012). arXiv:1210.3651
49. M. Blennow, P. Coloma, P. Huber, T. Schwetz, JHEP **1403**, 028 (2014). arXiv:1311.1822
50. G. Cowan, K. Cranmer, E. Gross, O. Vitells, Eur. Phys. J. C **71**, 1554 (2011). arXiv:1007.1727 [Erratum: Eur. Phys. J. C **73**, 2501 (2013)]
51. S.S. Wilks, Ann. Math. Stat. **9**, 60 (1938)
52. M. Blennow, P. Coloma, E. Fernandez-Martinez, JHEP **03**, 005 (2015). arXiv:1407.3274
53. J. Elevant, T. Schwetz, JHEP **09**, 016 (2015). arXiv:1506.07685
54. P. Coloma, A. Donini, E. Fernandez-Martinez, P. Hernandez, JHEP **1206**, 073 (2012). arXiv:1203.5651
55. R.A. Smith, E.J. Moniz, Nucl. Phys. B **43**, 605 (1972) [Erratum: Nucl. Phys. B **101**, 547 (1975)]